Md Rakin Tajwar

Phenomenological Heat Release Model for Multi-chamber Engines

School of Technology and Innovations
Master of Science in Technology
Master's Programme in Smart Energy

Vaasa 2024

UNIVERSITY OF VAASA
School of Technology and Innovations
Author: Md Rakin Tajwar
Title of the thesis: Phenomenological Heat Release Model for Multi-chamber Engines
Degree: Master's Programme in Smart Energy
Discipline: Master of Science in Technology
Supervisor: Maciej Mikulski, Amir Soleimani
Industrial Instructor: Ponnya Sein Hlaing
Year: 2024 **Pages:** 85

ABSTRACT :

To understand the detailed combustion trends of the internal combustion engine (ICE) for optimizing engine performance, accurate modeling of combustion phenomena is a crucial factor associated with ICE research. This thesis presents a phenomenological heat release rate (HRR) model for a pre-chamber combustion (PCC) engine to acquire insight into the combustion phenomena of the engine. The engine comprises two chambers which are PCC and main chamber combustion (MCC). The proposed model has been developed using a computationally efficient and flexible open-source Python framework that has been compared and validated against a 1-D simulated outcome of the GT-Power model.

The thesis proposes an approach for the thermodynamic heat release analysis of PCC and MCC, considering the in-cylinder pressure measurements from experimental data of both chambers. Both chambers estimate the residual mass, temperature, excess air-ratio lambda (λ), and initial specific heat capacity ratio (γ). Then, based on the initial γ, the bulk gas temperature, and crank-angle-based γ trace have been determined. Moreover, the heat losses have been determined by relying on convective heat transfer coefficients in both chambers. The first law of thermodynamics has been employed to calculate the HRR for PCC and MCC, the PCC also considers the mass transfer rate and enthalpy flow.

The proposed HRR model has been validated with the simulated output through comparison in three different loads (high, mid, and low). The various parameters of the proposed model including the temperature, heat transfer rate, specific heat capacity, heat loss, HRR, and cumulative HRR have been assessed by comparing the graphs of the developed model against the referenced model. Moreover, the model output has been validated using the mean absolute percentage error formula to ensure accuracy.

The model accurately computes the HRR and delivers promising results in the validation. The proposed HRR model offers faster computation than the referenced model, flexible adjustments, and modification of different parameters, and a more cost-effective solution than the simulated model since the GT model requires a high amount of licensing expense. Additionally, the model offers easy modification of the combustion process allowing for accurate tuning and optimizing over GT-Suite three-pressure analysis. Overall, the developed model accurately estimates the different parameters of the MCC's and PCC's HRR with fewer exceptions.

KEYWORDS: pre-chamber, cylinder pressure, combustion phase, phenomenological model, heat release, heat losses, specific heat capacity, cycle-to-cycle variability

Acknowledgement

This thesis was conducted in collaboration with Wärtsilä Corporation (R&D and Engineering, Advanced Concept team) and the University of Vaasa (UVA). I want to convey my heartfelt gratitude to all of those who have contributed outstanding input in this work to make this happen.

First of all, I would like to thank my thesis supervisor Maciej Mikulski, Professor, Energy Technology, for his steadfast guidance, notable feedback, and encouragement he provided throughout my thesis period. I want to express my deepest appreciation to my second supervisor, Amir Soleimani, Project Researcher, who has been my source of great support, advice, efforts, and time to help me overcome any challenge I faced. I am also grateful to my colleague Jeyoung Kim, Project Researcher, for his valuable input on the thesis work.

I am supremely grateful to my industrial instructor, Ponnya Sein Hlaing, Expert, Research Engine Performance, for his enormous efforts, superlative guidance, and great support for me who always pushes me to go the extra mile and keep me on track to accomplish the thesis. In addition, words of thanks go to my General Manager, Jari Hyvönen for believing in me giving paramount support and offering tremendous encouragement.

I am thankful to my parents Md Bashir Ahmed Chowdhury and Mst Noorjahan Begum who always believed in me and provided their best possible effort to support and guide me forward, without them achieving this milestone wouldn’t be possible for me. Moreover, I am grateful to my siblings for always loving, guiding, believing in me, and treating me as your baby brother. Particularly, a thank wouldn't be enough for my elder brother Sherjahan Ahmed Chowdhury Rajib for always holding me back and for unconditional support since childhood. I am in debt to all my family members, teachers, and friends to whom I am grateful forever.

Contents

Figures

Tables

Abbreviations

ICE	Internal Combustion Engine
PCC	Pre-chamber Combustion
MCC	Main Chamber Combustion
HRR	Heat Release Rate
PCSI	Pre-chamber Spark Ignition
CAD	Crank Angle Degree
CA	Crank Angle
CCV	Cycle-to-cycle Variability
SI	Spark Ignition
AFR	Air-fuel Ratio
BDC	Bottom Dead Centre
TDC	Top Dead Centre
SCE	Single Cylinder Engine
CVCC	Compound Vortex Controlled Combustion
PJC	Pulsed Jet Combustion
HAJI	Hydrogen-assisted Jet Ignition
WOT	Wide-open Throttle

TJI	Turbulent Jet Ignition
IVC	Inlet Valve Closure
EVC	Exhaust Valve Closure
EVO	Exhaust Valve Opening
GHG	Greenhouse gas
HC	Hydrocarbon
CO	Carbon Monoxide
LD	Light duty
H_2	Hydrogen
O_2	Oxygen
N_2	Nitrogen
AFR_{actual}	Actual Air-fuel Ratio
$AFR_{Stoichiometric}$	Stoichiometric Air-fuel Ratio
EU	European Union
EEA	European Environment Agency
W31	Wärtsilä 31
PM	Particulate matter
SG	Spark gas

Greek Letters

λ	Excess Air Ratio
γ	Specific Heat Capacity Ratio
ρ	Density
Θ	Crank angle degree
$\Delta P_{PCC\text{-}MCC}$	Pressure difference in the PCC

Other symbols

P	Pressure
m	Mass

Q	Heat release
U	Internal energy
h	Specific enthalpy
T	Temperature
V	Volume
R	Gas constant
V_{PCC}	Pre-chamber volume
V_d	Displacement volume
V_c	Clearance volume
h_g	Convective heat transfer coefficient

1 Introduction

1.1 Climate change and initiatives

Nowadays, the focus on climate change has been continually increasing due to regulatory pressure. To address the climate concerns, rules and regulations are being revised to pressure companies and governments alike to reduce carbon emission. The European Union(EU)'s strategy of decarbonization to achieve net zero emissions entails that the substitution of petroleum and coal with alternative forms of energy is required to eliminate carbon emissions entirely (European Commission & Directorate-General for Climate Action, 2019).

In accordance with the European Environment Agency (EEA), over the last decades, the EU implemented significant actions to tackle climate change, resulting in a reduction of roughly 31% of EU emissions in the year 2022 compared to 1990 scales. The major reason behind this is the rise of deploying alternative sources of energy as well as the mitigation of utilizing fossil fuels. Additionally, EEA is aiming for aspiring goals of mitigating greenhouse gas (GHG) emissions by approximately 55% or close to this at the end of the current decade. Moreover, the European Union (EU) targeted to become carbon-neutral with net zero GHG emissions in the year 2050. Achieving these aims is set up to reduce emissions by transitioning from fossil-based sources to eco-clean energy (Climate Change Mitigation: Reducing Emissions, 2024).

1.2 Advancements in internal combustion engine

The internal combustion engine (ICE) plays a significant role in modern life since it is fuelling up various sectors of the global economy. In the transportation field, ICE is predominantly involved in facilitating the movements of goods and services while driving the connection between the nations and communities. In 2022, the ICE technology accounts for over 99.8% of the world's transportation sector (G. Kalghatgi et al., 2022).

Additionally, ICEs are the integral part and primary driving force of powering technologies within the transport industry. ICEs have been the driving force of marine propulsion systems over the years, fuelling a substantial portion of the world's shipping sector as well as in the power generation sector. Despite the growing interest in sustainable energy sources (for instance, electric propulsion and fuel cells), ICEs remain the most reliable option for performing vital aspects in the field of marine transportation owing to their dependability, vast existing infrastructure, and greater power density (Aabo, 2020). Despite the recent developments in automotive industry, for instance battery integration in electric vehicles, the dominance of the ICE is still there in the transportation field. One of the drawbacks of electrification is the life-cycle carbon footprint of battery systems, which account for the energy employed in generating power and battery production. It discloses that their actual advantages are less compared to the initial perceptions (Reitz et al., 2020). Furthermore, Reitz et al. (2020) pointed out that large-scale implementation of new electrification infrastructure for battery-driven systems will require critical design changes, sophisticated control mechanisms, and substantial amounts of raw materials handling via mining. However, the limited availability of essential materials is limiting the scope of building an ICE-less energy solution. It is expected that the ICEs will remain in the market due to their highly efficient large-scale manufacturability (G. T. Kalghatgi, 2015).

On the other hand, it is evident that one of the major factors causing the rise of global warming is the consumption of fossil fuels. Specifically, the ICE is responsible for GHG emissions, particularly carbon dioxide emissions, because of the combustion of petroleum gasoline in the ICEs (United Nations, 2022). Moreover, ICEs generate emissions such as hydrocarbon (HC), carbon monoxide (CO) and particulate matter owing to the incomplete combustion fuel (Sane et al., 2014).

The press for improving efficiency and adapting sustainable fuels ICEs is pushed forward by climate protection goals and gradually rigorous pollutant emissions control guidelines.

Balmelli et al. (2024) pointed out that this is especially crucial while considering the difficulty to electrify sectors such as maritime, heavy-duty, stationary, on and off-road vehicles, including the combined generated power. Furthermore, they also addressed that the implementation of high-efficiency ICEs that are powered by sustainable fuels, for instance, hydrogen (H_2), ammonia, biogenic and synthetic methane, as well as other alternative fuels, has notable significance. Moreover, alternative fuel exploration, engine design optimization, employing hybridization and power systems are the prime examples of these strategies. By deploying these initiatives, it is indeed possible to mitigate CO_2 emissions to a considerable extent (Leach et al., 2020).

The importance of the natural gas as an alternative fuel is growing rapidly with regards to petrol oils used in the ICEs because of a wide range of causes, as it requires little preprocessing before utilizing it. Currently, natural gas accounts for well over 35% of electricity consumption in the U.S. Furthermore, in terms of the diesel and gasoline fuels generating emissions corresponding to 25%-30% more energy because of their high hydrocarbon ratio (Rajasegar et al., 2021; Roethlisberger & Favrat, 2002).

Lean burn combustion has the ability to attain higher engine efficiency as it has a higher specific heat capacity ratio in the air-fuel mixture. Moreover, this lean burn method mitigates heat transfer loss due to the lower combustion gas temperatures leading to the rise in efficiency while also reducing the NOx emissions. Additionally, this system allows for reduction of engine knocking while allowing higher engine load operation (Rajasegar et al., 2021). Moreover, these enhancements are attained by operating the engine with a lean air-fuel mixture by using the excess air ratio (λ).

The primary impediment, however, stems from the limited flammability of the most fuels. This is why it leads to instability in combustion and heightened emissions of CO and unburned hydrocarbons (UHC). Operating with an averaged excess air ratio (λ) above 1.4 in a standard spark ignition (SI) engine is going to exhibit unsatisfactory cycle-to-cycle

variability (CCV) (Tang et al., 2022). For addressing the downsides of lean burn combustion, pre-chamber spark ignition (PCSI) concept emerged as a viable solution, leading to the development of highly performing SI engines (Garcia-Oliver et al., 2021).

1.3 Prechamber combustion concepts

The pre-chamber combustion (PCC) is a technological breakthrough that has strong potential for the forthcoming low carbon fuelled engines. The PCC system is a small chamber separated from the main chamber combustion (MCC); the PCC assembly includes a spark plug and jet nozzle that exits to the MCC via multiple small nozzle orifices (Tang et al., 2022). Furthermore, the pre-mixed charge contained in an either passive or active-fuelled PCC is usually ignited by the spark plug in PCSI systems (Rajasegar et al., 2021). Moreover, the actively fuelled system employs a particular fuel injection system within the PCC that maintains the air-fuel ratio (AFR) to an optimal level for combusting lean air-fuel charge in the MCC (Novella et al., 2023). While the passively fuelled system does not use any auxiliary fuel injection system in which the fuel-air mixture is ingested from MCC during the compression stroke. The concept of employing the PCC system is to release rapid, hot and reactive jets from PCC to MCC mixtures (Tang et al., 2022).

The PCSI system initiates combustion at distinct places within the MCC by employing turbulent jets of hot products, which result in an enhancement in combustion rates (Attard, William P. & Blaxill, Hugh, 2011; Attard, William P. et al., 2010). Thus, the burning phase can be enhanced to increase thermal efficiency under operating conditions, while allowing optimal spark timing thanks to improved knock resistance (Attard & Blaxill, 2012).

Despite not being able to have ultra-lean combustion, passive systems still improve engine performance via extending the knocking limits, enhancing combustion efficiency and stability of the combustion in comparison to typical SI engines (Trombley & Toulson, 2023). According to Garcia-Oliver et al. (2021), the prime benefits of PCC in power sta-

tions and transportation fields, specifically the active ones with PCC fuel injection systems, include lesser CCV, which leads to knock reduction, allowing an increased in compression ratio (CR) to enhance engine efficiency.

1.4 Phenomenological models

To observe the combustion phenomena, including the heat release rate (HRR), heat losses, ignition timing, and CCV, a phenomenological model is a viable solution to demonstrate the complex process of combustion. These parameters are estimated while focusing on the experimental information rather than mainly on theoretical aspects. In engine studies, the phenomenological HRR model is an observed model, based on measured data and empirical correlations. These models are usually simpler to obtain and have more descriptive combustion behaviour. By, employing assumptions depending on the measured data to estimate complex combustion behaviour (Barba et al., 2000).

The necessity for phenomenological models has been introduced due to the complex combustion process, usually very intricate to model from the core theoretical aspects. Moreover, using phenomenological HRR provides additional dimension to the measured data rather than qualitative understanding. Also, these models allow simpler control and monitoring of the combustion phase, enabling changes relying on experimental characteristics in place of critical calculations.

2 The problem statement

HRR analysis is a vital method for post-process combustion trends, getting insight into the rate and quantity of the heat released during combustion that aids in enhancing engine performance. Wärtsilä has to employ the HRR model frequently, and there are different solutions for developing the HRR model in different platforms, such as GT-Suite and MATLAB data post-processing. However, each software comes with the burden of a high amount of licensing costs and lengthier computation times. These issues open up the scope for introducing a practical solution, with the following objectives

- Objective 1: Implement a phenomenological HRR model for multi-chamber engine using an open-source programming platform. The model should be able to conclude the HRR estimation below 90 seconds on a standard PCC platform, making it suitable for Wärtsilä W31 SG single cylinder engine (SCE).
- Objective 2: Test the functionality of the developed HRR model based on three operating points of the Wartsila 31SG SCE. The testing matrix should involve different engine loads and lambda values, and the parameter should be validated considering mean absolute error. The functionality analysis should cover gross HRR, heat losses, instantaneous gamma, cumulative HRR, mean gas temperature, and lambda values at spark timing.
- Objective 3: Validate the model quantitively against reference three pressure analysis model (TPA) implemented in GT-Suite Software.

2.1 Thesis architecture

The study has been categorized into six core chapters, which include an introduction, problem statement, theoretical framework, methodology, results and discussions, conclusions. Chapter one outlines advancements in ICE, the phenomenological HRR model, and the PCC system. Chapter two provides the problem statement with the constructive objective. Chapter three is a comprehensive analysis of existing literature, emphasizing

PCC solutions and their combustion phenomena and reviewing HRR calculation methods. Conversely, in chapter four, the methodology entails the method by which the HRR model is built and how measured experimental data is employed in the HRR calculation. Next, the fifth chapter provides the descriptive details of the HRR model including the results of the different parameters with validation and thorough discussions. In chapter six, the thesis is concluded by summarising the outcomes of this research.

3 Theoretical framework

Accurately estimating the HRR in ICEs is fundamental in perceiving the combustion phenomena, engine efficiency, and performance estimation. In multi-chamber engines, the complex interactions between the PCC and MCC necessitate further refinement over the well-accustomed conventional HRR calculations. The objective of this chapter is to explore the past history of PCC systems, including their utilization in production engines, and the existing HRR calculation methods for these kinds of systems.

3.1 Evolution of pre-chamber systems

The PCC system has been in use from the early part of the 20th century, and this system consisted of a 2-stroke Ricardo Dolphin engine in which combustion initiated in the PCC cavities. As per Figure 1, a passive inlet valve was used to conduct the fuel-rich mixture into the PCC. Afterward, this rich mixture was first ignited in the PCC, generating hot combustion jets that then ignited the leaner mixture in the MCC, which was the very first introduction of PCC technology (Ricardo, 1922).

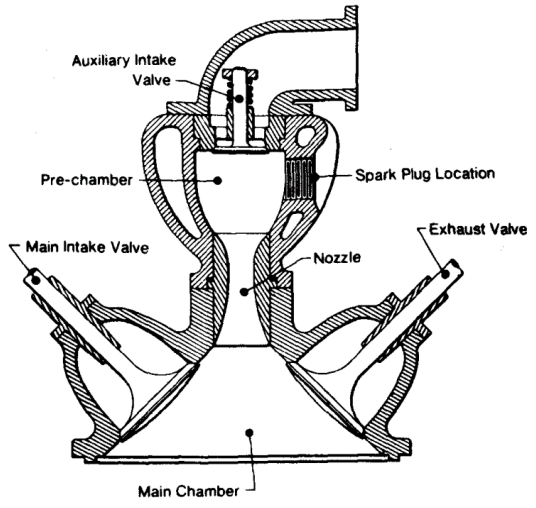

Figure 1. Design of Cylinder Head in the Ricardo Two-Stroke Stratified Engine (Ricardo, 1922)

Ricardo invented and patented the separated chamber concept as a three-valve stratified charge engine, demonstrated in Figure 1. The invention employed a single carburettor to deliver the rich mixture in the PCC, whereas only air was initiated in the MCC. The output power was controlled by varying the rich air-fuel mixture that were supplied through a throttle in the intake manifold.

Ricardo's 3 valve stratified engine design also inspired different divided chamber concepts by other researchers in their patents (A. Bagnulo, 1947; Mallory, 1938). Mallory, (1938), patented a two-stage PCC system, which introduces a particular system that ignite a rich mixture before pushing them into the MCC as shown in Figure 2. This was a semi-diesel system, avoiding the need for a high diesel CR.

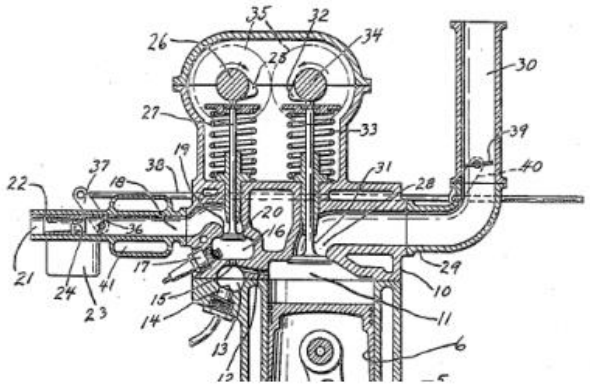

Figure 2. Mallory's Two-stage PCC systems (Mallory, 1938)

In another study A. Bagnulo, (1947) deployed a stratified design within the PCC to govern the energy release rate in the PCC system (Figure 3). The system has a high swirl in the PCC with compression via tangent nozzle position. The torch cell engine concepts were also developed from the formula of the 2-stroke Ricardo Dolphin engine, and these systems were implemented by automakers like Toyota, Ford, and Volkswagen. These systems have proven effectiveness in extending the lean operating range of engines (Brandstetter, 1980; Adams, Tim G., 1979; Noguchi, M. et al., 1976).

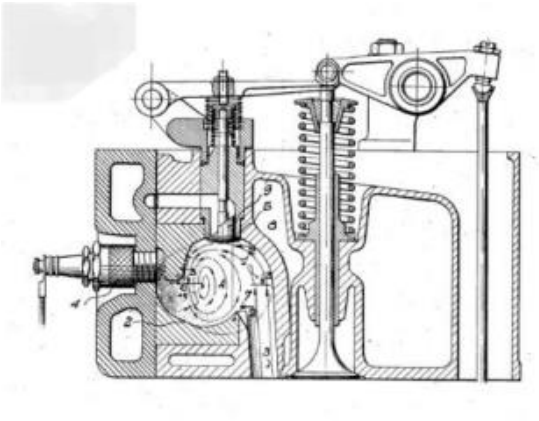

Figure 3. Bangulo's Stratified Mixture Engine Design (A. Bagnulo, 1947)

Among the PCC technologies, one of the most prominent achievements is Honda's Compound Vortex Controlled Combustion (CVCC) system. This system has been implemented to conform the 1975 emission standards without the need for a catalytic converter, as depicted in Figure 4. The system consisting of an over-fuelled PCC that ignites a fuel-rich cloud and leaner mixture in the MCC leads to decreasing the emissions and enhancing the high fuel efficiency (Date et al., 1974).

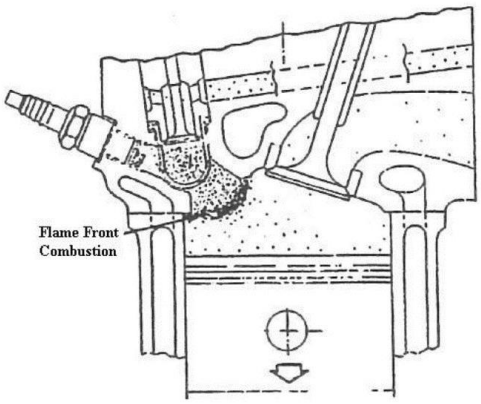

Figure 4. Honda's Flame Torch-Based Ignition System in the CVCC Engine (Date et al., 1974)

One of the great technological advancements in PCC systems was the L.A.G. process, introduced by L. A. Gussak (Gussak, L. A. et al., 1975) and collaborators (Figure 5). More-

over, they introduced various investigations to observe the consequence of fuel-rich mixture combustion in the PCC over MCC. From their experiments, they considered a PCC size of 2-3% of the engine clearance volume and an orifice opening area ratio of 0.03-0.04 cm^2/cm^3 of PCC volume. The orifice length was recommended as 50% of its diameter for an ideal balance between engine efficiency and emission performance. In another study, the L.A.G. system was incorporated in the Volga passenger vehicle, employing a cam-actuated injector to supply a rich ($\lambda = 0.5$) mixture into the PCC, resulting in an ultra-lean ignition ($\lambda = 2$) mixture in the combustion chamber (Gussak et al., 1983).

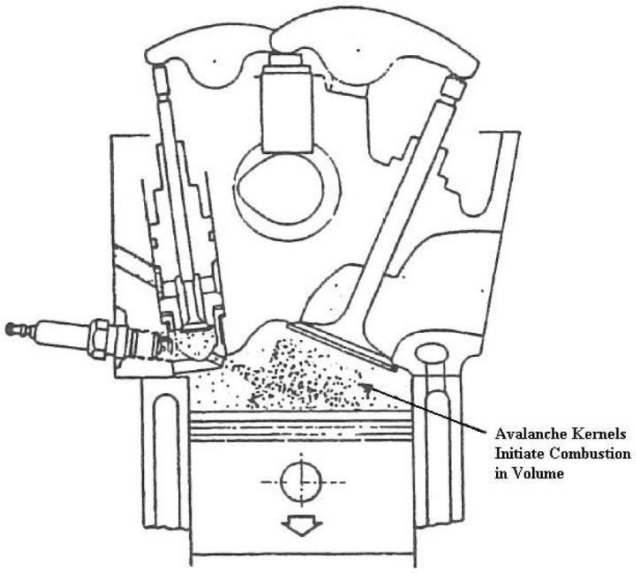

Figure 5. LAG Ignition System: Active Radicals for Distributed Flame Ignition

In another study, the L.A.G. system incorporated within the Volga passenger vehicle, employing a cam-actuated injector to supply a rich ($\lambda = 0.5$) mixture into the PCC, resulting in an ultra-lean ignition ($\lambda = 2$) mixture in the combustion chamber (Gussak et al., 1983).

In the 1980s, Oppenheim's pulsed jet combustion (PJC) is introduced while emphasizing developing large eddies of the air-fuel mixtures in the MCC for enhancing the mixing, combustion, and fuel efficiency. But this invention just marginally raised the dilution limits, generating higher amounts of hydrocarbon (HC) and CO emissions (Oppenheim et al., 1989).

Another study demonstrated that in the 1990s, the hydrogen-assisted jet ignition (HAJI) system was introduced (Watson, 1997). This employs a small quantity of H_2, approximately 2% of the main fuel energy injected into the PCC, to produce a rich mixture. Consequently, the PCC generates turbulent jets, which stimulate ultra-lean combustion in the MCC and extend it lean limit to $\lambda = 5$ at wide-open throttle (WOT) (Dober, 1999). IAV and MULTITORCH have implemented a PCC system equipped with a spark plug with pilot injection, exhibiting the employ of H_2 as a PCC fuel leading to extend the dilution limit of the MCC to $\lambda = 2$ (Getzlaff et al., 2007).

In case of recent developments, the turbulent jet ignition (TJI) system by Mahle Powertrain has enhanced fuel economy and mitigated emissions, whereas elevating the dilution limit to $\lambda = 2$ and ensuring stability at low ignition energy (Attard & Blaxill, 2012).
In-depth studies have been conducted on active and passive TJI systems by MAHLE Powertrain, whereas Maserati has employed passive TJI in high-performance SI engines. MAHLE Powertrain and Maserati have shown that TJI systems may increase the CR. This is possible due to the improved knock resistance these systems offer, which also leads to better overall cycle efficiency (Trombley & Toulson, 2023). According to Attard & Blaxill (2012), the MAHLE TJI system offers significant advantages across various operating modes in a SCE using PCC. This concept is implemented for light-duty (LD) engines that employ gasoline. The TJI resulted in attaining 42% of peak brake efficiency while enhancing the fuel economy by 20% when running in lean conditions ($\lambda > 2.0$). Additionally, with this engine condition, the system achieves single-digit engine-out NOx emissions. Moreover, mitigating knocking in TJI allowed for an appropriate advances of spark timing, which facilitates the adequate combustion phasing. Proper combustion phasing leads to improvements in the engine's work output, which consequently increases the engine efficiency with the same volume of fuel (Attard & Blaxill, 2012).

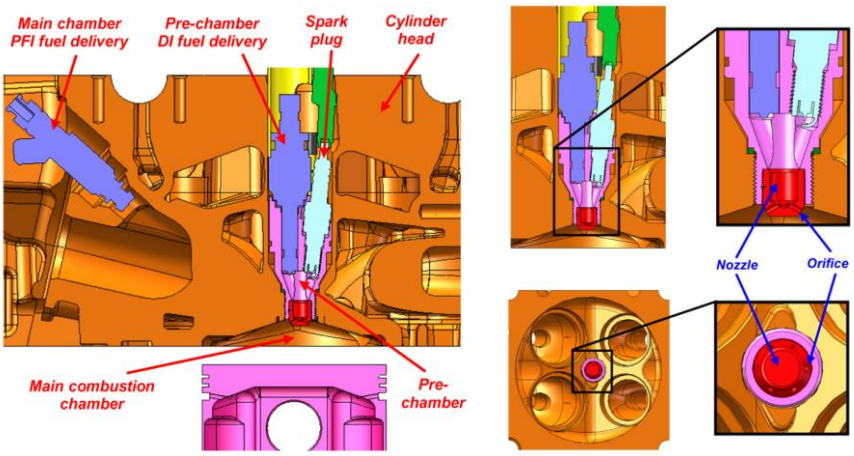

Figure 6. Section and Design View of the MAHLE's TJI System with Central Pre-Chamber and Nozzle in a Four-Valve Pent-Roof Combustion Engine (Attard & Blaxill, 2012).

3.2 Fundamental concepts of pre-chamber spark ignition

A PCSI is typically a small cavity that is commonly placed in the cylinder head just above the MCC. This entire system constitutes about 3-5% of the clearance volume in total (Silva et al., 2020), however Gussak et al. (1983) suggest it should be closer to 2-3%. The combustion system begins with igniting the air-fuel mixture in the PCC, typically accomplished via a spark plug. With regards to the PCC tip, there are multiple nozzle holes interacting between the MCC and PCC. Following the spark discharge, the PCC combustion products flow into the MCC and in the form of jets, where they function as multiple ignition sites, depending on the number of nozzle holes. Conversely, the typical SI engines employ only one igniting source of a spark plug (Rajasegar et al., 2021; Alvarez et al., 2018; Toulson et al., 2010). The researchers also stated that the PCSI system provides comparatively a simpler alternative to a conventional system that requires only minor or no changes in the engine. Employing PCC that generates turbulent jets to enhance the combustion efficiency also enables improved ignition without requiring major engine restructuring or critical modifications (Rajasegar et al., 2021).

As previously discussed in Chapter One, PCC systems can typically be categorized into two distinct forms: active and passive PCC. As per Rajasegar et al. (2021), in an actively

fuelled PCC system, the auxiliary fuel injector aids in maintaining near-stoichiometric conditions in the PCC regardless of the MCC charge composition. Moreover, the active fuelling systems provide an extra level of flexibility by allowing the PCC to be operated at a rich fuel-air mixture. Subsequently, the jets operate at higher temperatures to help ignite the lean mixtures in the MCC, however richer PCC lambda does not mean that the jets will be hotter. A mixture that is too rich in PCC would even extinguish the flames. The jets will improve the turbulence mixing process in the MCC. All these factors contribute to the effective ignition of the lean charge in the MCC. Regarding the passive PCC system, the fuel-air mixture is delivered only to the MCC, and then the PCC ingests from the PCC mixture during the compression stroke (Tang et al., 2022). In a passive case, although not having an auxiliary fuel injector mitigates the system complexity, there is a lack of direct control of the charge composition in the PCC.

To understand the combustion phenomena of a multi-chamber engine, it is required to calculate the HRR. HRR sheds light on how energy is released during combustion. First, it demonstrates the rate at which the jets from the PCC ignite a leaner mixture in the MCC, enabling accurate adjustment of spark timing to enhance engine efficiency and adjust fuel consumption based on the requirement. The HRR method aids in identifying combustion anomalies, including knocking or misfires, allowing for appropriate alterations to enhance the stability.

3.3 Phenomenological heat release model

The HRR works as an indicating factor of the combustion process, which provides an understanding of the combustion behaviour and process. It is obtained from the experimental data, which consists of the cylinder pressure. This measured the rate of energy released in the course of the combustion process. However, HRR is not a tool for simulating the combustion; rather, it is a powerful post-processing analysis tool employed to evaluate combustion performance depending on the measured data. To simulate the combustion process in this model, it is required to estimate parameters such as the tem-

perature, air-fuel mixing, specific heat capacity and heat transfer rate in order to determine the gross HRR. Gross HRR is defined as the total energy released in combustion, while the net HRR is the amount of heat released, which also includes losses taking place predominantly with cylinder walls. The phenomenological models offer the benefits of efficient computation (Rezaei et al., 2016). Furthermore, the zero-dimensional single zone model is typically employed to analyse engine performance based on experimental data.

According to the Barba et al. (1999) who developed a high-speed engine model that primarily operates by employing a combustion engine rate. The employed model illustrates the variations in HRR using an experiment that depends upon a particular reference point. The core concepts of the phenomenological model lie in determining the governing physical and chemical phenomena. In addition, it demonstrates the concepts of physical-based models as well as empirical formulas relying on the experimental data (Barba et al., 2000). Researchers also stated that the phenomenological concepts are relatively cost-effective in terms of computation timing, which enables the model to consider the various parameters analysed, which include injection timing, main injection duration, pilot injection timing, and duration of it. The calibration of the phenomenological model is relatively straightforward with only a few parameters required to be associated with the experimental data. Consequently, this approach allowed for the measurement of HRR characteristics, giving a crucial understanding of vital parameters, which include peak pressure, engine efficiency, and combustion noise.

The next part will provide a comprehensive overview of HRR estimations of these two chambers in a broader approach and existing research work in this field.

3.4 Heat release rate estimations

The HRR estimation is influenced by distinct parameters, including the wall heat loss, presumed gas properties, crank angle (CA) resolution, and used noise mitigation methods (Ceviz & Kaymaz, 2005). In terms of HRR estimation, the specific heat capacity ratio is the crucial thermodynamic parameter (Gatowski et al., 1984).

According to Ceviz & Kaymaz (2005), assuming the in-cylinder charge has a constant mass period from inlet valve closure (IVC) to exhaust valve closure (EVC), the first law of thermodynamics may be applied for an incremental CA interval expressed as equation (1),

$$dQ_{hr} = dW + dU_s + dQ_W \tag{1}$$

where, dQ_{hr} refers as the gross HRR because of combustion, dW represents the change of work, dU_s is the changes in sensible internal energy and dQ_W represents the energy transfer from charge to cylinder wall.

Furthermore, the subsequent equations can be addressed this way: Equation (2) indicates the work done by the system while a small volume change occurs at constant pressure.

$$pdV = dW \tag{2}$$

where p refers to assumed constant pressure, and dV is the change in volume.

The change in sensible internal energy is expressed in equation (3),

$$mc_v dT = dU_s \tag{3}$$

where, m refers to mass, c_v is the specific heat at constant volume, and dT represents the change in temperature.

The ideal gas law is expressed in differential form in equation (4),

$$\frac{d(pV)}{mR} = dT \tag{4}$$

where, R is the specific gas constant.

The specific heat capacity ratio (γ) is outlines in equation (5):

$$\frac{R}{c_v} = \gamma - 1 \tag{5}$$

here, γ is the specific heat capacity ratio at constant pressure c_p to specific heat at constant volume c_v.

To derive the typical form of the HRR equation, substitute equation (2) to equation (5) into the equation (1) as well as restructuring the variable. This subsequently provides the typical format of the first law HRR equation.

$$dQ_{hr} = \frac{\gamma}{\gamma - 1} PdV + \frac{1}{\gamma - 1} VdP + dQ_W \tag{6}$$

where, dQ_{hr} refers to the gross HRR, γ represents the specific heat capacity ratio, dV and dP are the change in volume and pressure respectively. dQ_W is the energy transfer to the cylinder wall.

There are distinct factors has been considered for estimating the HRR to perceive the insight of combustion phenomena, this includes the factors like specific heat capacity ratio, cylinder pressure, chamber volume, in-cylinder temperature, and heat losses. Here,

the specific heat capacity ratio is crucial for estimating the HRR. There are several methods available for estimating the gamma; one such method is the method as stated by Brunt et al. (1998). In this method, gamma was considered as a function of temperature in the heat capacity ratio. Besides this, gamma (γ) likewise relies on the equivalence ratio (ϕ), and the repercussion of overlooking this factor results in an inaccurate HRR calculation. In another study, the gamma is estimated based on the NASA polynomial coefficient formula (Smith et al., 1999). The specific heats can also be estimated using the Zucrow & Hoffman (1976).The study is going to employ the NASA polynomial coefficient formula to determine the specific heat capacity ratio.

In terms of calculating the heat transfer, different approaches have been introduced over the past. According to Hohenberg (1979), who mentioned that the heat transfer in ICEs are principally affected by convection, the fundamental factors he derived from the law of similarity for turbulent tube flow and defined the heat transfer coefficient, which leads to calculating the heat transfer rate. Woschni (1967) developed a model for estimating heat transfer coefficients for ICE based on the laws of similarity driving convective heat transfer, which contains the piston motion convection and convection because of combustion. Moreover, this leads to a universal equation for estimating the heat transfer coefficients, which in turn provides the heat transfer rate. In another study, despite the inapplicability due to the phase lag among gas temperature and heat flux changes, the notion of instantaneous heat transfer coefficient could be employed in analysing the heat transfer in ICE (Annand, 1963).

The HRR is typically termed the rate at which the fuel's chemical energy is released during combustion (Alvarez et al., 2018). In engine studies, researchers have extensively investigated the HRR as a parameter in combustion method research. Among these research works, Sakai et al. (1974) conducted a study as depicted in Figure 3 is considered one of the primary ones on this approach.

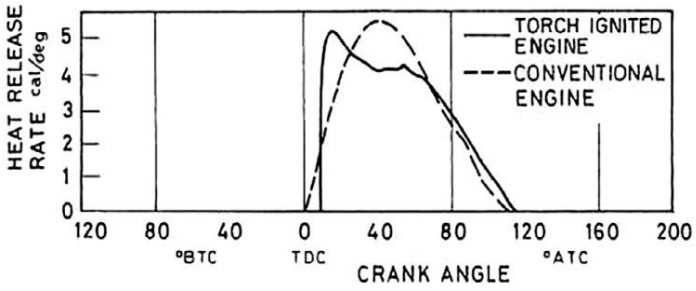

Figure 7. Combustion characteristics comparison at constant indicated specific fuel consumption (Sakai et al., 1974)

Figure 7 depicts that the combustion process exhibits a swift elevation of HRR in the PCC during the starting phase and exhibits an early sudden peak in the HRR, followed by a steady fall. In typical engines, the HRR commonly conforms to a bell-shaped curve; however, the researchers pointed out that within a PCC, the air-fuel ratio has a substantial impact on the initial peak of PCC HRR. In contrast, in a torch-ignited engine, as per Figure 7, the peak value of the HRR declines and approximately corresponds to the typical engine as the mixture becomes leaner (Alvarez et al., 2018).

In another study (Ryu et al., 1987), the similar HRR characteristics was perceived for different connecting holes diameters between the PCC and the MCC. For the narrow diameter, the HRR constant patch reported by Sakai et al. (1974) was not observed and only the peak resulting from the initial combustion phase appears to be attributed to high-speed combustion. They also point out that HRR increases progressively since there is significant turbulence caused by the torch jet impacting the piston crown.

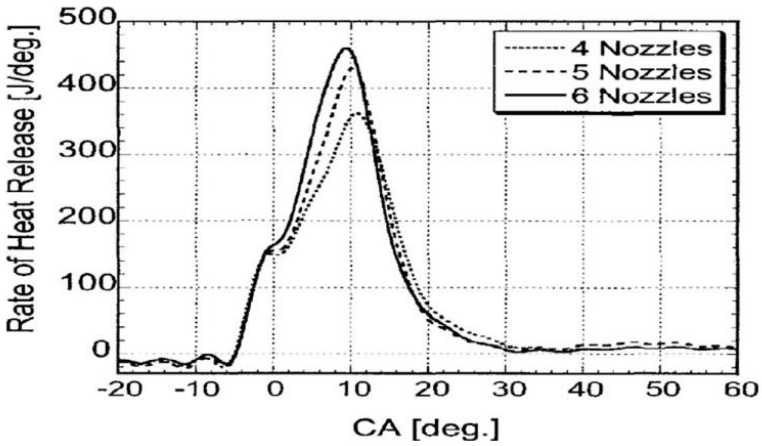

Figure 8. Rate of Heat Release Comparison in the Main Chamber (Kawabata, Yasuharu & Mori, Daichi, 2004)

Furthermore, in a separate research work, the researchers addressed that employing increasing quantity of nozzles led to reduced HRR as per the Figure 8 (Alvarez et al., 2018; Kawabata, Yasuharu & Mori, Daichi, 2004).

4 Methodology

4.1 The object

In this research work, a multi-chamber single-cylinder medium-speed 4-stroke engine from Wärtsilä is used. This base engine is the W31SG, a PCC spark gas (SG) engine designed by Wärtsilä specifically for pure gas operation in lean-burn conditions, the considered operating points of this engine are taken from the SCE. The Wärtsilä SG concept deploys a PCC to increase stable ignition and combustion efficiency, which allows it to be a well-suited high-efficiency application. The advanced interactive functionality allows for thorough combustion assessment. The employed engine takes part in mitigating the environmental footprint by setting a benchmark in fuel efficiency and emission performance.

Here are some of the of the main technical details of this engine as outlined below:

Table 1. Wärtsilä 31 SG engine technical data

Parameter	Specification
Cylinder Number	1
Cylinder bore	310 mm
Piston stroke	430 mm
Engine speed	750 rpm
Displacement Volume	32 dm^3

Table 1 demonstrates the technical details of the W31 SG which consists of a SCE with gas-only configuration. Table 1 contains vital engine parameters that involve cylinder bore, piston stroke, engine speed, and displacement volume. The crucial aspect influencing the research is the method of pressure measurement. The employed engine of this study is equipped with Kistler sensors to monitor the key parameters of the two chambers MCC, and PCC. The pressure transducer for MCC is a Kistler Type 6124A piezoelectric cylinder pressure sensor which is located near the periphery. The sensitivity of the 6124A sensor is -30 pC/bar and the thermal sensitivity shift is ≤±1 throughout the

temperature range, and the Kistler Type 6052CU is set for PCC close to the roof of the PCC. The PCC sensor contains -20 pC/bar sensitivity and temperature variation is ≤ ± 0.5 within 200 ±50^{0}C. The study measured the airflow and fuel flow to get the lambda.

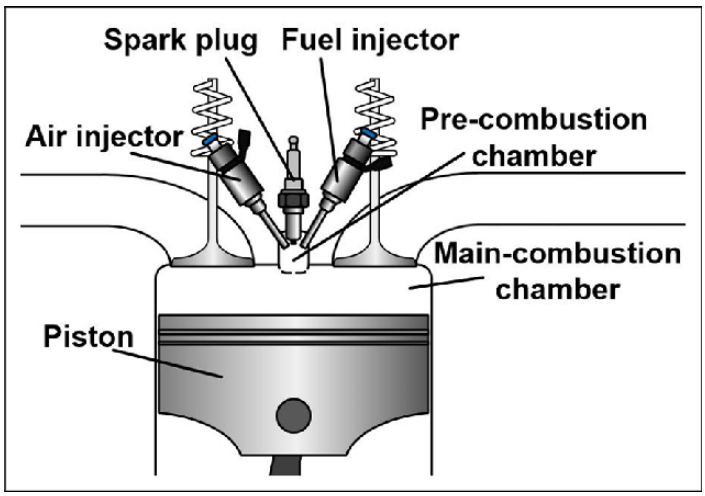

Figure 9. Turbulent jet ignition engine structure (Song et al., 2017)

Figure 9 provides the fundamental structure of the TJI SCE. To acquire a better mixing within the PCC, the TJI employs gas in the PCC system. However, this is not practicable in liquid fuel systems as it is needed dual-fuel mechanisms and this led to difficulty, intricate operating mechanisms, and expense (Song et al., 2017). The SG engine is an SI lean burn engine, within the intake stroke of the SG engine, the gas-air mixing before the inlet-valve within the intake stroke this mixture, and employs a spark plug for igniting the small amount of mixture in the PCC gas-air mixture, which is richer than the MCC and flows through the intake ports. During the compression stroke, both the richer PCC gas-air mixture and MCC gas-air mixture are compressed. As per the combustion stroke, at the end of the compression phase, the flame from the PCC nozzle after-ward ignites the leaner gas-air mixture within the MCC which results in faster combustion trends. With regards to the expansion stroke, throwing out the combusted gas from the chamber by the exhaust valve opening (EVO). Then the whole process begins again within the intake stroke. The SG engine injects the fuel via the port fuel injection system and operates

independently for each cylinder. The cylinder operation of a cross-section of the SG engine's cylinder and demonstrates that the gas injected within the PCC is on the left, and the port fuel gas injection is on the right side. The SG engine conducts lean burn operation, which leads to a reduction in mean in-cylinder temperature in comparison with diesel engine operation (Smulter, 2016).

4.2 The HRR model for multi-chamber combustion

The section outlines the HRR analysis of a multi-chamber engine sequentially through a flowchart outlined in Figure 10. The implementation was based primarily by the method proposed by Hlaing (2022). The method initiates with determining the residual mass and initial gamma for PCC and MCC. Next, determine the lambda estimation and followed by the gas temperature and specific heat capacity ratio for PCC and MCC. Afterward, it determines the heat losses relying upon the convective heat transfer coefficient and then calculating HRR for PCC and MCC. The HRR starts with estimating the mass transfer rate, and the study employed the PCC mass transfer model from flow through a nozzle equation of Heywood (2018). Moreover, to conduct mass calculations the study uses the instantaneous CR model from Shah et al. (2012).

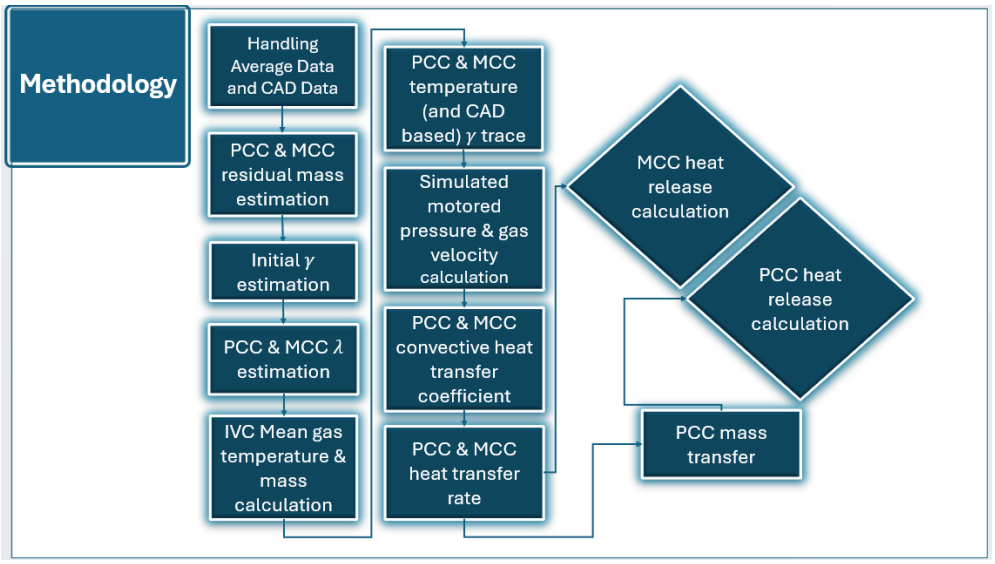

Figure 10. SCE multi-chamber engine HRR Model Flowchart

The flowchart (Figure 10) begins with extracting recorded test data from the SCE. Each test data point consists of averaged, and crank-angle based data. The latter includes data streams such as both the MCC and PCC pressure traces, as well as the CA array for 300 cycles. The averaged data consists mainly of moving-averaged values of testbed parameters such as gas flow rates, intake and exhaust temperatures and ignition timings for a recorded duration of 3 minutes. The next step in the study is to estimate the residual mass and then the initial gamma, which will help with later calculations of the gas temperatures and crank-angle-based specific heat capacity ratio (γ) trace for both the PCC and MCC. The following step is to determine the mean in-cylinder gas temperature, which will lead to calculating the temperature and gamma-based specific heat capacity ratio for the PCC and MCC. The next step in the process is calculating the heat transfer rate for both the PCC and MCC. Subsequently, we calculate the HRRs for the MCC and PCC, and based on these rates, we estimate the gross HRR. Lastly, various outputs of the HRR analysis can be visualized using a dedicated script. In the upcoming subsections of this chapter, each of the steps will be thoroughly addressed in detail.

4.3 Handling average data and crank angle-based data

The process begins with the data acquisition, where the averaged data and crank angle-based data are taken from experimental performance files and AVL Indicom files, respectively, that have been gathered from the Wärtsilä engine. Additionally, the performance file contains the averaged data, temperature data, fuel types and engine power rates, and engine geometry. Moreover, AVL Indicom files comprise in-cylinder pressure traces. The AVL Indicom file has extracted traces using Catool, which initially generated a MAT file from the AVL Indicom files. Then, by loading the MAT file extract the CA resolution and calculate the average cylinder pressure. Before extracting the data, we sort it into distinct groups for ease of data identification for subsequent analysis.

4.4 Residual mass estimation

The residual gas fractions (x_{res}) are typically referred to as the ratio of the residual gas mass and the total mass. According to Heywood (2018), the x_{res} is commonly estimated the combustion chamber within the compression stroke. Moreover, the residual gas fractions by virtue of the valve overlap backflow can be stated as expressed in equation (7),

$$x_{res,backflow} = \int \frac{m_{exh}}{\rho_a V_d [(r_c + 1)/r_c]} \frac{1}{6N} dt \tag{7}$$

where, $x_{res,backflow}$ refers to the residual gas fraction due to backflow, m_{exh} represents the exhaust gas masses, ρ_a is the air density, V_d displacement volume, r_c refers to the CR, and *N* represents the engine speed. The equation incorporates exhaust gas masses within time while considering the air density, CR, and displacement volume for measuring the residual gas fraction upon the valve overlap backflow.

Now, the total residual gas mass fraction become which outlined in equation (8):

$$x_{res} = x_{res,IVO} + x_{res,backflow} \tag{8}$$

Here, x_{res} represents the total residual gas fraction after inlet valve closure, and $x_{res,IVO}$ refers to the residual gas fraction at inlet valve opening (IVO). The residual mass can be estimated by employing the equation (9):

$$m_{res} = \frac{m_{fa} \times X_{res}}{1 - X_{res}} \tag{9}$$

where, m_{tot} refers to the total mass at IVC, which is basically the mass flow into cylinder per cycle, m_{res} is the residual mass, and X_{res} is the residual gas mass fraction.

Estimating the lambda is vital for understanding the combustion characteristics, which directly affect the fuel's burn rate, including the efficiency of the combustion phenomena. Determining the lambda based on the instantaneous CR model from Shah et al. (2012) as excess air ratio addressed in equation (10).

$$\lambda = \frac{AFR_{actual}}{AFR_{stoichiometric}} \tag{10}$$

where, AFR_{actual} is the actual air-fuel ratio and $AFR_{stoichiometric}$ refers as the stoichiometric air-fuel ratio.

The mass of the air-fuel mixture trapped in the cylinder at the IVC of the PCC is also crucial for perceiving the PCC phenomena. This study estimates the mass of gas at the start of the combustion while considering the in-cylinder pressure, in-cylinder temperature, and volume of the combustion chamber to estimate trapped mass in the PCC. As per the lambda in the PCC, this treatment is to assess how much of the injected fuel (active fuelling) is captured by the PCC, and the PCC will always leak out some fuel into the MCC during the early injection in the intake stroke. The scavenging ratio (0.77) is applied to the mass of gas in the PCC, which leads to providing the trapped mass of the air-fuel mixture. The PCC trapped mass gas has been estimated below in equation (11).

$$m_{gas\ trap\ PCC} = m_{gas\ PCC} \times PCC_{SR} \tag{11}$$

where $m_{gas\ trap\ PCC}$ refers to the actual trapped fuel in PCC, $m_{gas\ PCC}$ denoted as the gas flow into PCC via and PCC_{SR} is the scavenging ratio at PCC. Additionally, for the lambda estimation of MCC, scavenging ratio has also been applied to determine the trapped air-fuel ratio in MCC, although the effect on MCC air-fuel ratio is minimal.

Ideal gas equation was used in estimating the mass of trapped air in the PCC at IVC and as per the equation (12),

$$m_{air\ trap\ PCC} = \frac{mean(P_{PCP} \times 1e^5)}{R_{air} T_{PCC}} V_{air\ trap\ PCC} \quad (12)$$

Now, calculating mass fraction of gas and air of PCC at IVC expressed in equation (13,14, and 15)

$$m_{tot\ trap\ PCC} = m_{gas\ trap\ PCC} + m_{air\ trap\ PCC} \quad (13)$$

$$m_{frac\ gas\ PCC} = \frac{m_{gas\ trap\ PCC}}{m_{tot\ trap\ PCC}} \quad (14)$$

$$m_{frac\ air\ PCC} = \frac{m_{air\ trap\ PCC}}{m_{tot\ trap\ PCC}} \quad (15)$$

where, $m_{air\ trap\ PCC}$ refers to the mass of trapped air in PCC at IVC, $m_{tot\ trap\ PCC}$ represents the total mass trapped in PCC at IVC and $m_{frac\ gas\ PCC}$ mass fraction of gas in PCC at IVC.

Now estimating the lambda for the instantaneous compression ratio (ICR) model as per Shah et al. (2012) at IVC based on cylinder pressure data and assuming the scavenging ratio (0.77) of PCC for late injection.

Determining the density of the MCC will lead to the total mass of the PCC as stated in equation (16 and 17) respectively,

$$\rho_{MCC} = \frac{P_{MCP}}{R_{air} T_{g\ MCC}} \quad (16)$$

$$m_{tot\ PCC\ ICR} = \rho_{MCC} \times V_1 \quad (17)$$

where, R_{air} is the gas constant of air, $T_{g\ MCC}$ refers to the mean in-cylinder temperature for MCC, ρ_{MCC} is the density of the MCC and V_1 denotes as the ingress volume from MCC in the PCC which is calculated as expressed in equation (18).

$$V_1 = V_{PCC}\frac{\varepsilon - 1}{\varepsilon} \tag{18}$$

Here, V_{PCC} refers to the initial volume of PCC, and ε represents the ICR. The ingress volume from MCC in the PCC (V_1) is a key factor as it directly affects the total mass estimation within the PCC.

Again, for mass of air at IVC as showed in equation (19),

$$m_{air\ PCC\ ICR} = m_{tot\ PCC\ ICR} + m_{frac\ air\ MCC} \tag{19}$$

where, $m_{frac\ air\ MCC}$ is the mass fraction of air in MCC at IVC which has been calculated similar to the $m_{frac\ air\ PCC}$.

Now the equation(20) becomes,

$$m_{gas\ PCC\ ICR} = m_{tot\ PCC\ ICR} \times m_{frac\ gas\ MCC} \tag{20}$$

where, total mass in PCC and mass fraction of mass gas at IVC,

$$\lambda_{PCC\ ICR} = \frac{\left(m_{air\ trap\ PCC} + m_{air\ PCC\ ICR}\right)}{\frac{\left(\frac{m_{gas\ trap\ PCC}}{m_{gas\ PCC\ ICR}}\right)}{AFR_{stoichiometric}}} \tag{21}$$

As per the equation (21) where $AFR_{stoichiometric}$ is the stoichiometric air-fuel ratio, $m_{air\ trap\ PCC}$ is the mass of trapped air in PCC at IVC and $m_{air\ PCC\ ICR}$ refers to the mass of air in PCC at IVC, $m_{gas\ trap\ PCC}$ is the mass of trapped gas in PCC, and $m_{gas\ PCC\ ICR}$ is the mass of gas in PCC at IVC.

Similarly, employing this formula for the MCC to estimate the lambda for MCC at IVC,

$$m_{tot\ MCC\ ICR} = m_{tot\ trap\ MCC} - m_{tot\ PCC\ ICR} \quad (22)$$

where $m_{tot\ trap\ MCC}$ is the total trapped mass in MCC at IVC and $m_{tot\ PCC\ ICR}$ denotes as the total trapped mass in PCC at IVC.

$$m_{air\ MCC\ ICR} = m_{air\ trap\ MCC} - m_{air\ PCC\ ICR} \quad (23)$$

where $m_{air\ trap\ MCC}$ refers to the trapped mass of air in MCC at spark timing and $m_{air\ PCC\ ICR}$ mass of air at spark timing in PCC.

$$m_{gas\ MCC\ ICR} = m_{gas\ trap\ MCC} - m_{gas\ PCC\ ICR} \quad (24)$$

$$\lambda_{MCC\ ICR} = \frac{\left(m_{air\ trap\ MCC} + m_{air\ MCC\ ICR}\right)}{\frac{\left(m_{gas\ trap\ MCC} + m_{gas\ MCC\ ICR}\right)}{AFR_{stoichiometric}}} \quad (25)$$

Here, $\lambda_{MCC\ ICR}$ represents the lambda of MCC at spark timing, $m_{tot\ MCC\ ICR}$ is the total mass in MCC at spark timing, $m_{air\ MCC\ ICR}$ refers to the mass of air in MCC at spark timing and $m_{gas\ MCC\ ICR}$ is the mass of in MCC at spark timing.

According to Heywood (2018), the in-cylinder pressure at different crank angle degree (CAD) during the compression and expansion strokes of an engine's running cycle may be used to obtain the HRR. The research works apply the first law of thermodynamics to describe the energy transfer in the in-cylinder charge during the non-flow, constant mass period between IVC and EVC.

4.5 Initial gamma estimation

Following the structured sequence as depicted in Figure 10, this section follows up the initial gamma estimation by employing the NASA polynomial coefficient. In this study, we utilized a NASA polynomial coefficient formula, extracting the polynomials used in

the thermodynamic properties within the GRI30 chemical kinetics mechanism (Smith et al., 1999). This combustion study is built for different fuels, despite the method's applicability to other fuel types such as natural gases. We estimate the specific heat capacity at a constant pressure of oxygen (O_2), nitrogen (N_2), and H_2 using the following formula for the low-temperature range, which is below 1000K, as it allows for a straightforward, accurate calculation by mitigating the complex molecular adjustments that are predominant at high temperatures as outlined in equation (26),

$$C_{p\ gas} = \frac{A + BT + CT^2 + DT^3 + ET^4 R}{M_{gas}} \tag{26}$$

where *A, B, C, D,* and *E* are the numerical coefficients, *T* is the initial temperature, M_{gas} is the molecular weight of the gas and *R* is the gas constant. Equation (26) defines the specific heat constants for the constant pressure of considered gas $C_{p\ gas}$ as a function of temperature and numerical coefficients. To measure the specific heat capacity of a gas mixture, we employ Equation (27), which calculates the specific heat capacity of a gas mixture based on the specific heat capacities and masses of the individual components:

$$C_p = C_{p\,gas}\left(\frac{m_{gas}}{(m_{gas} + m_{air})}\right) + C_{p\,air}\left(\frac{m_{air}}{(m_{gas} + m_{air})}\right) \tag{27}$$

Here, m_{gas} refers to the mass of the gas, m_{air} is the mass of air, and $C_{p\,air}$ is the constant air pressure. While Equation (26) specific heat capacity of gas at constant pressure, Equation (27) applies this to a gas mixture, considering the contributions of both gas and air. The masses are commonly considered constant in these equations. For determining the specific heat capacity at constant volume Equation (28) is expressed as

$$C_v = C_p - R_s \tag{28}$$

where, R_s is the specific gas constant and now estimating the gamma based on the lower temperature(1000K) becomes Equation (29) becomes,

$$\gamma_{in} = \frac{C_p}{C_v} \tag{29}$$

where γ_{in} refers to the initial gamma. Using this formula of initial gamma estimation, the initial gamma of PCC and MCC has been estimated in this study. In the upcoming subsection, the mean gas temperature variable of both PCC and MCC will be addressed.

4.6 Mean gas temperature of PCC and MCC

The mean gas temperature variable is a critical aspect of the HRR analysis, as it facilitates estimating the temperature and crank angle-based gamma trace, heat transfer rate and, resulting in estimating HRR calculation. This variable assists in determining the temperature at a particular point in between the closing of the intake valve and the opening of the exhaust valve. To determine the mean in-cylinder gas temperature, it requires the temperature at the IVC for both PCC and MCC.

As per polytropic process, stated by Wray et al. (1997), here calculating the temperature between IVC and exhaust valve opening (EVO) as expressed in equation (30):

$$T_g = P_{PCC,\ MCC} V_{PCC,\ MCC} \frac{1}{nR} \tag{30}$$

where, $P_{PCC,\ MCC}$ and $V_{PCC,\ MCC}$ refer to the PCC & MCC pressure and volume respectively, *n* is the polytropic index, and *R* is the gas constant assumed to remain constant the equation (31) becomes:

$$T_g = P_{PCC,\ MCC} V_{PCC,\ MCC} \frac{T_{IVC}}{P_{IVC} V_{IVC}} \tag{31}$$

where, T_g is the mean gas temperature for the PCC and MCC at IVC and EVO. P is the pressure in the PCC and MCC. V denotes the combustion volume, and the temperature at the inlet valve closing timing is T_{IVC}.

4.7 Instantaneous gamma estimation for the PCC and the MCC

According to Brunt et al. (1998), the specific heat capacity ratio is denoted as gamma (γ) at constant pressure and volume respectively (C_p/C_v). C_p refers to the specific heat capacity at the constant pressure is the required heat quantity to raise the temperature at constant pressure and similarly, C_v represents the required heat to raise the temperature at constant volume. Underestimated gamma ratios lead to high HRR values during the combustion and will result in a negative HRR values after combustion. This research work estimated the initial gamma and the mean gas temperature variable of it which leads to calculation of γ trace of the PCC and MCC. Using the initial gamma (γ_{in}) and the mean gas temperature variable while calculating the temperature and crank-angle based gamma trace for PCC & MCC as demonstrated by Brunt et al. (1998).

$$\gamma = \gamma_{in} - 6e^{-5}T_g + 1e^{-8}T_g^2 \tag{32}$$

where, γ_{in} is the initial gamma and T_g is the mean gas temperature variable.

4.8 Heat transfer calculation for PCC and MCC

To determine the HRR, the heat transfer was steady-flow forced-convection, the heat flux transferred to a solid surface while the heat flux is outlined using the equation (33):

$$\frac{dQ_{ht}}{dt} = A_w\left(T_g - T_{wall}\right) \tag{33}$$

where, h_c is the convective heat transfer coefficient, T_g refers to the mean gas temperature that is calculated employing ideal gas law, T_{wall} represents the cylinder wall temperature, and A is the instantaneous heat transfer surface area of the combustion chamber. The heat transfer coefficient has been determined by employing the Woschni (1967) model. This coefficient has been expressed in equation (34) as per Woschni's model.

$$h_c(W/m^2K) = 3.26B(m)^{-0.2}p(kPa)^{0.8}T(K)^{-0.55}w(m/s)^{0.8} \quad (34)$$

Here, the h_c is the convective heat transfer coefficient, B refers to the cylinder bore, p represents the cylinder pressure measured in kPa while the other parameters have been outlined in the SI unit system, T is the cylinder temperature and w is the average gas velocity. The average gas velocity has been calculated based on Woschni's formula according to Heywood (2018) at IVC and EVO shown in equation (35).

$$w = C_1\bar{S}_p + C_2\frac{V_dT_{IVC}}{P_{IVC}V_{IVC}}(P_f - P_m) \quad (35)$$

where, V_d refers to the displacement volume, P_f represents the instantaneous cylinder pressure, P_m is the motored cylinder pressure within the same CA, $\bar{S}_p$ denotes the mean piston speed, P_{IVC}, V_{IVC}, and T_{IVC} working fluid pressure, volume, and temperature at IVC, C_1 and C_2 are constants employed to consider different values at different cyclic period (Heywood, 2018).

4.9 Mass transfer between the PCC and MCC

In PCC engines, the mass transferring between the PCC and MCC happens continuously within the entire cycle. For estimating the mass transfer, employ the nozzle flow equation introduced by Heywood (2018). The equation is assumed to have steady-state flow through the nozzle. The mass transfer formula adapts the turbulent flow via the discharge coefficient.

$$\frac{dm}{dt} = \frac{C_d A_t P_{PCC\ MCC}}{\sqrt{RT_g}} \left(\frac{P_{MCC\ PCC}}{P_{PCC\ MCC}}\right)^{\frac{1}{\gamma_{PCC}}} \left[\frac{2\gamma}{\gamma - 1}\left(1 - \left(\frac{P_{MCC\ PCC}}{P_{PCC\ MCC}}\right)^{\frac{\gamma-1}{\gamma}}\right)\right]^{\frac{1}{2}} \quad (36)$$

As per the Equation (36), the C_d denotes to the discharge coefficient value of the nozzle, A_t refers to the cross-sectional area of the nozzle and γ is the specific heat capacity ratio, $P_{PCC\ MCC}$ is the PCC and MCC pressure traces. The mass flow and direction of the flow for PCC and MCC has been calculated based on the pressure difference of the two chambers. Moreover, considering the forward flow direction particularly during the mass flows from the PCC to the MCC it has been solved using exact same manner of equation (36).

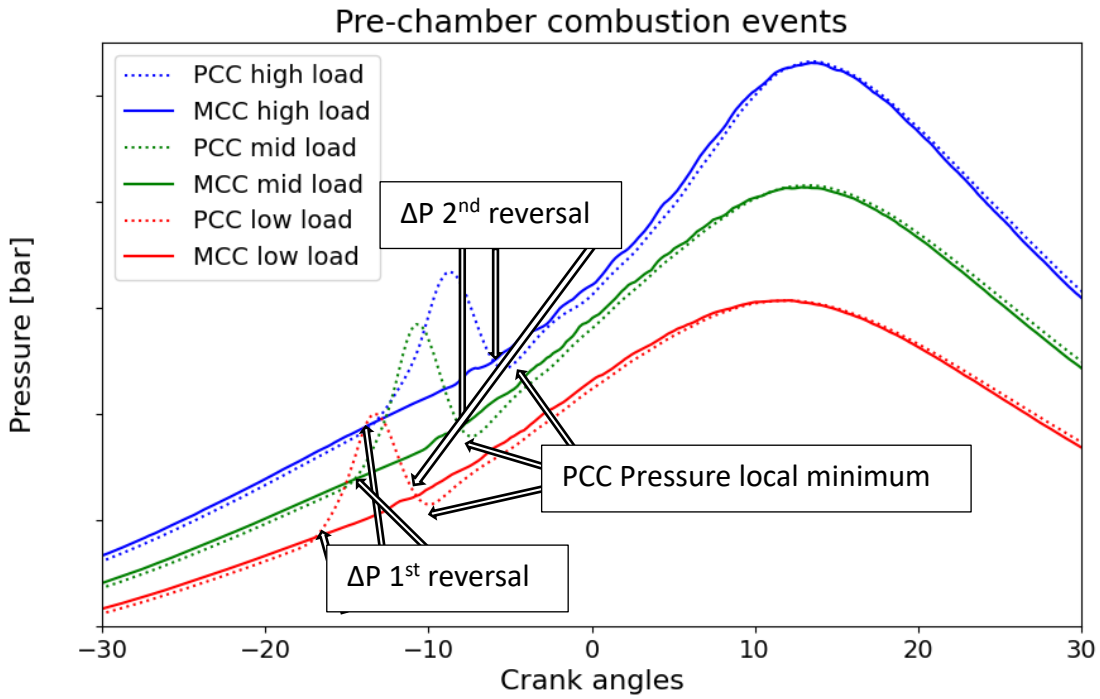

Figure 11. Events of Pre-chamber combustion

Figure. 11 shows the PCC combustion events considering three operating loads (high, mid, and low). After spark plug ignition in the PCC, the PCC pressure increases above the MCC pressure at a certain CA. There is a gradual increase of pressure value in the PCC as combustion advances and the pressure differential between the PCC and MCC reaches

the maximum pressure value which is termed ($\Delta P_{PCC\text{-}MCC}$) as it is the pressure difference of both the chambers. The first introduction of pressure in the PCC is higher than in the MCC, referred to as pressure differences reversal 1 (ΔPR_1), and in the second case after the maximum pressure difference ($\Delta P_{PCC\text{-}MCC}$) is referred to as ($\Delta PR_2$). As it can be pointed out the local minimum of PCC pressure does not correspond, because of the flow momentum, the PCC continues to discharge slightly beyond the peak of the ΔPR_2 (Hlaing, 2022).

4.10 Heat release calculation for PCC and MCC

By substituting equation (1) of appendix (1) to equation (3) of appendix (1) onto equation (38) as well as rearranging the variable, it provides the typical format of the HRR equation for the MCC and the PCC subsequently.

$$\frac{1}{\gamma-1}V_{MCC}\frac{dP_{MCC}}{dt}+\frac{1}{\gamma-1}P_{MCC}\frac{dV_{MCC}}{dt}=\frac{dQ_{MCC}}{dt}-P_{MCC}\frac{dV}{dt}+h_{\frac{PCC}{MCC}}\frac{dm}{dt} \tag{37}$$

$$\frac{dQ_{MCC}}{dt}=\frac{1}{\gamma-1}V_{MCC}\frac{dP_{MCC}}{dt}+\frac{\gamma}{\gamma-1}P_{MCC}\frac{dV_{MCC}}{dt}-h_{\frac{PCC}{MCC}}\frac{dm}{dt} \tag{38}$$

$$\frac{dQ_{PCC}}{dt}=\frac{1}{\gamma-1}V_{PCC}\frac{dP_{PCC}}{dt}+h_{\frac{PCC}{MCC}}\frac{dm}{dt} \tag{39}$$

For an incremental CA interval, the first law of thermodynamics can be formulated for this period as the gross HRR formula while considering both on the PCC and MCC.

$$\frac{dQ_{gross\ hr,MC}}{d\theta} = \frac{1}{\gamma - 1} V_{MCC} \frac{dP_{MCC}}{d\theta} + \frac{\gamma}{\gamma - 1} P_{MCC} \frac{dV_{MCC}}{d\theta} - C_p T_{PCC,MCC} \frac{dm}{d\theta} + dQ_{ht} \quad (40)$$

$$\frac{dQ_{gross\ hr,PC}}{d\theta} = \frac{1}{\gamma - 1} V_{PC} \frac{dP_{PC}}{d\theta} + C_p T_{PCC,MCC} \frac{dm}{d\theta} + dQ_{ht} \quad (41)$$

when the derivative of $\frac{dm}{d\theta}$ is positive meaning that there is flow from the PCC to MCC and vice versa. In a typical engine with a single combustion chamber, the trapped mass may be assumed to remain constant during the IVC and EVO, rather simplifying the mean gas temperature calculation. While considering the PCC engines, the trapped mass in PCC and MCC differs with every crank revolution. This difference indicates that the mean gas temperature estimations may not fully take effect of mass transfer. However, for simplification, the quantity of mass of air-fuel from MCC to PCC is assumed to be negligible, resulting in allowing gas temperature estimation using the ideal gas equation.

4.11 Code structure

The analysis code has been written in the Python 3.12.4 environment. In this work, Python libraries such as NumPy, Pandas, Scikit-Learn, Matplotlib and SciPy have been employed. This development has been carried out in a structured manner, where the method has been segmented into multiple sub-models, which resulted in the final HRR model for the PCC and MCC. The model has been outlined as per Figure 12, in which there are six major sub-scripts with dedicated functions. As stated in Figure 12, the main script is the front-end part of the code where different calculation functions can be called depending on the necessity. As per the addressed sections 4.3 and 4.5 here, where we implement those processes in Python code. Specifically, section 4.3, the averaged data and the crank angle-based data have been structured in the engine test data retrieval script, and this script is designed to organize and store averaged data and crank angle-based data, along with fundamental engine geometrical parameters to ensure efficient

sorting and facilitate particular parameters to be readily accessible for further computation

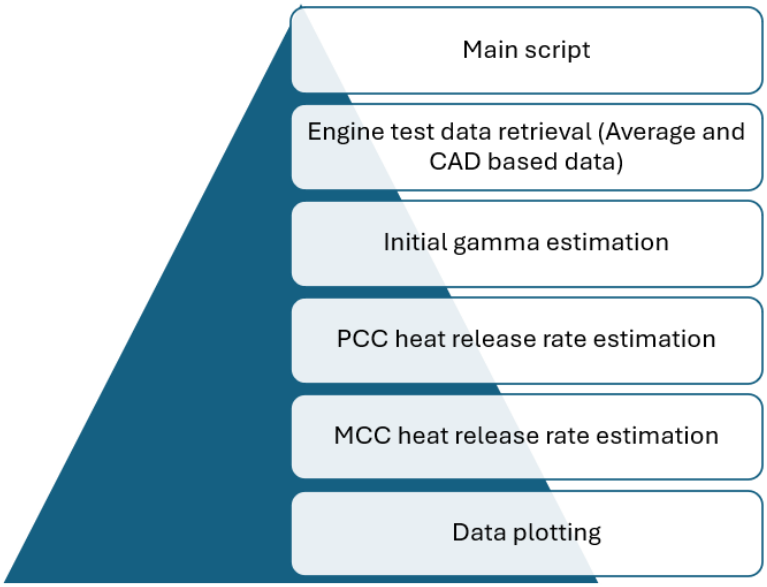

Figure 12. Code structure of the phenomenological HRR model

The initial gamma estimation, outlined in section 4.5, is estimated employing NASA polynomial coefficients within the initial gamma calculation script. In terms of estimating the gamma tracing in the MCC and PCC, the initial gamma calculation enables accurate gamma tracing and ensures the estimated outputs are easily accessible in other parts of the scripts for subsequent estimation.

There are two different sub-scripts for both the PCC and MCC for HRR scripts, the primary structure of the script initiated with estimating the residual mass from the previous cycle. The required geometrical parameters and averaged data have been initialized in the scripts from the output of (load raw data script). In the next part of the code, the trapped mass at IVC was calculated for PCC and MCC, respectively followed by the mean gas temperature and gamma trace estimation. Later part of the scripts provides a simulated motored pressure trace and gas velocity for the heat transfer rate using the Woschni correlation. With all the required inputs now being calculated, of the final part of the scripts estimating the net HRR.

In PCC script, an additional part is included to estimate the mass transfer between the PCC and MCC. This mass transfer rate leads to the enthalpy transfer rate calculation between the two chambers, since this parameter is important for the accuracy of the PCC HRR calculation. Finally, the gross HRR is calculated for the PCC. Both the PCC and MCC HRR script also provide cyclic data of 5, 25, 50, 75 and 90% heat release angles as well as the combustion duration for all 300 cycles included in the test file. In both the MCC and PCC scripts, using the structure method, all the calculated data output has been managed and stored in three different categories: instantaneous values, cyclic values, and mean values. Then, these structured data outputs have been saved in pickle file format for data retrieval.

The final script of this code structure is the data plotting scripts, where the different parameters of MCC and PCC such as mean in-cylinder temperature, gamma tracing, lambda tracing, gross HRR, cumulative HRR and heat transfer rate are illustrated along with the single cycle calibrated GT-power output data of same datapoints. This script provides a clear comparison between the two separated files which include the structured pickle file, and the GT-Power extracted text file through visualization implementation. It considers the mean value high-load, mid-load and low-load data results from 300 engine cycles, along with the single cycle value of the simulated data output from the GT-post file. Moreover, the main tasks of the data plotting scripts involve generating different plots for all the important parameters such as the mean gas temperature, heat transfer rate, gross HRR, and cumulative HRR against the CAD.

4.12 GT power-based engine model for performance comparison

This research compares the results of the developed HRR model with those of the GT-Power model. GT-Suite is an eminent software application widely employed by engine manufacturers to measure different aspects of engine and vehicle efficiency such as fuel consumption, power output, and engine emissions. The software system involves GT-Power, an engine development environment for the transient and steady-state modelling of an arbitrary ICE (Gamma Technologies).

Figure 13 shows the 1-D model of the W31 single-cylinder SG engine developed in GT-POWER software and the thorough engine geometry of it including the intake and exhaust parameters. Fig. 13 The GT-power model employed a three-pressure analysis (TPA) approach, as the method has the potential to make a connection within engine testing and simulation to deliver thorough combustion analysis, gas exchange analysis, and validating measured data. The TPA method employs intake pressure, cylinder pressure, and exhaust pressure to determine the gaseous exchanges and combustion. Moreover, analysing the combustion solely relies on the cylinder pressure employing enforced trapped conditions. Additionally, the TPA approach enables to conduct the comparison and calibration of predictive combustion with measured data (Cylinder Pressure Analysis - Gamma Technologies).

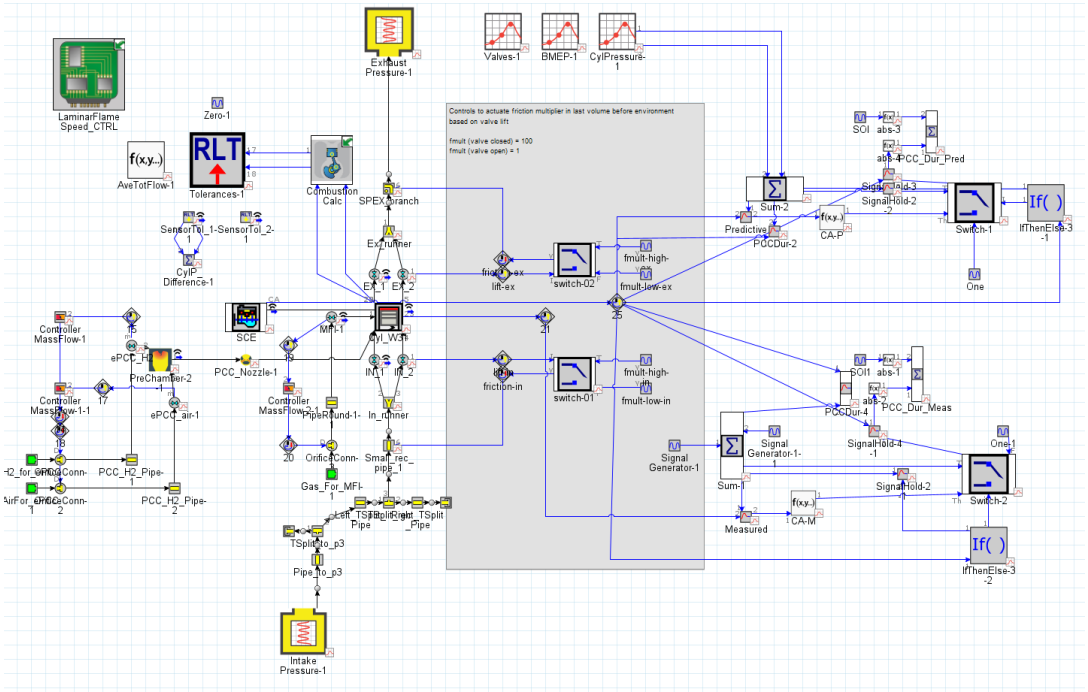

Figure 13. The 1-D GT Power W31 engine setup

The reference GT model operated the commonly employed TPA method operating at steady-state conditions and considering only single-cycle simulation data. Based on the pressure traces, the PCC and the MCC apparent gross HRR have been estimated as single-

zone assumptions. Moreover, the MCC heat transfer rate of the GT model has been calculated using the Woschni GT model, however, the PCC employed the flow equation to determine the PCC heat transfer rate, that initially calculated the gas velocity to estimate convective heat transfer coefficients via the Colburn analogy (Gamma Technologies).

In this research work, to validate the developed HRR model in Python platform, results from a GTPower simulations model, internally developed withing Wärtsilä RDE was used. Results from a specific test data point calculated using the multi-chamber HRR analysis code was compared against the GT simulation results of the same test point of three different loads.

The output data extracted from the GT-post file of this simulation result includes the gross HRR, heat transfer rate, cumulative HRR, specific heat capacity ratio, lambda trace, and mean gas temperature variable. In order to conduct the validation of these code results from this HRR model, we have extracted the simulated HRR model of GT-post file data of the same experimental file.

4.13 Scope and methods of validation

The proposed HRR model has been validated against employing a GT-Power model. The GT-POWER model utilized the three-pressure analysis model and experimental data to simulate the HRR. To compare and validate the developed HRR model, this GT-simulated model was employed as a reference model. For estimating the errors and discrepancies between the Python-developed model and the GT model mean absolute percentage error (MAPE) method has been used to determine the error percentage. There have been three different operating points considered for the validation of starting with high load, mid load, and low load operations to assess the model's variability. This also allows for analyzing the operating functionality of the Python-developed model and opens up the scope for further improvement.

5 Results and discussion

This chapter will demonstrate the comparison and validation of the HRR model results of this research against the simulation output from GT-Power. The referenced GT-power model has considered the TPA formula to estimate the HRR. There have been differences in the calculation of the implemented model of the research work and the referenced GT model. In terms of the heat losses, the PCC model used a flow equation while the developed model of the research work used the Woschni heat transfer calculations which may result in some discrepancies in the results. However, in both models, the MCC heat transfer calculations used the Woschni model. The data points of GT-power results have been extracted from GT-post in text format and the implemented model result also extracts the structured data points in pickle format. These two data files of three different loads (high, mid, and low) for different parameters have been compared in this chapter and later the compared results have been validated using the MAPE formula. As the employed engine is a PCC engine that contains two chambers, MCC and PCC, this research work will compare the results of both chambers between the Python script and the GT output.

The deployed engine in this research is a four-stroke engine, and one operating cycle contains 720 degrees, which is two revolutions. The degrees have been specified as CAD between -360 to 360, with 0 degree placed at firing TDC, in which the different strokes can be differentiated/specified. The intake stroke of the engine starts from -360 to -180 CAD, compression strokes between -180 to 0 CAD, expansion strokes between 0 to 180 CAD, and the exhaust strokes from 180 to 360 CAD. The comparison of the HRR data for the studied model and the partially tuned GT-Power simulation results has been conducted as a function of CA.

This remaining part of this chapter will present the extent to which indeed the developed model is comparable towards the tune GT model with the aid of graphical representations, comparing differences, and identifying areas of enhancement. Lastly, the Y-axis

ticks of every graphical representation of this chapter have been kept hidden for confidentiality.

5.1 Calibration of the reference GT-power model

It is crucial to conduct the validation of the predicted results of the GT-power with the experimental data to assure the accuracy and tuning of the reference model in the combustion analysis. The Python model is developed in a way that allows for running on different kinds of fuels ensuring its capabilities to handle distinct applications. For validating the study, the research particularly emphasizes employing H_2 as a fuel. The H_2 offers a clean source of energy and allows for net zero carbon emissions goals for a sustainable future. The employed data points introduced in the study are calibrated and tuned for H_2 combustion, ensuring a thorough evaluation of the Python-implemented model's performance and accuracy. As the model is built in the TPA method, we initially compare the PCC and MCC cylinder pressure to ensure the tuning of the simulated GT model. Moreover, it also compares the logarithmic pressure-volume behaviour of the predictive GT results with the experimental data to ensure the robustness of the simulation.

Figure 14 demonstrates the three loads of experimental PCC pressure traces against the CADs for conducting the PCC HRR analysis. The dotted (blue, green, and red) lines indicate the high, mid, and low loads provide the gathered averaged PCC experimental pressure data for over 300 cycles in the analyzed Python HRR model, and the solid lines indicate the captured single-cycle high, mid, and low loads data of GT-power simulations based on the same experimental measured output using the TPA method. The colour combination remains the same for the other parameters where Python output is stated in dotted lines while GT data remain the solid lines. It is observed that from the acquired high-load experimental pressure data the calibrated GT-model also captured traces with slight differences in it. The mid-load and low captured values of the GT models show slightly lower values at their peak.

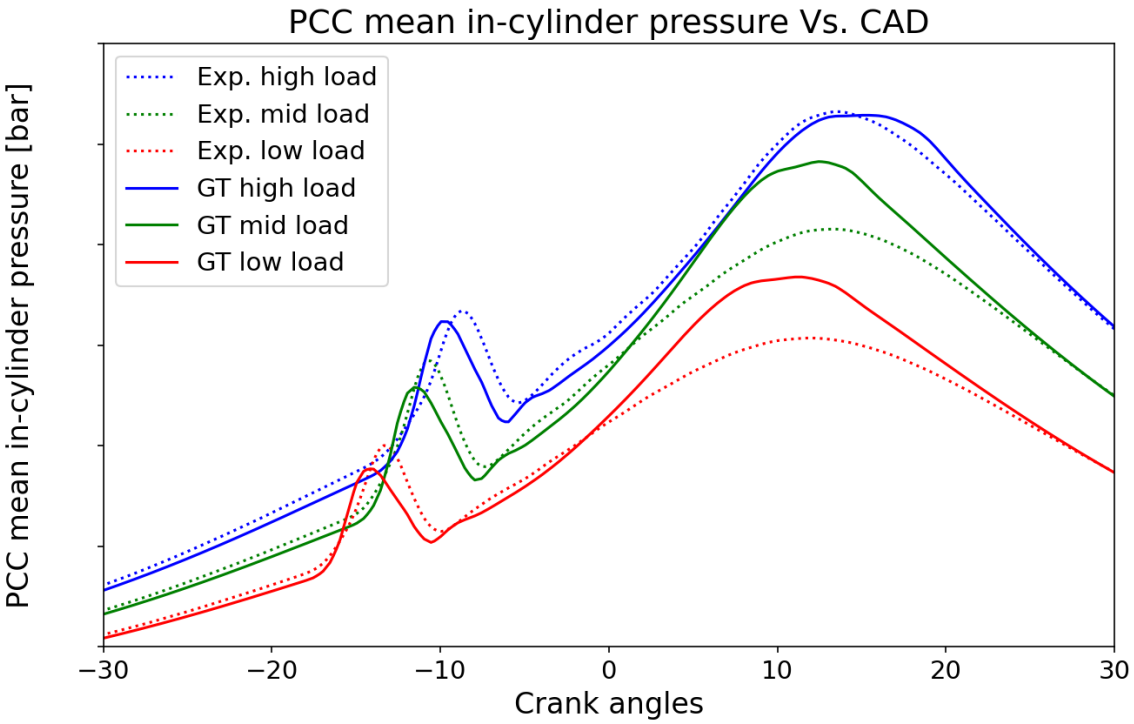

Figure 14. PCC in-cylinder pressure with crank angle

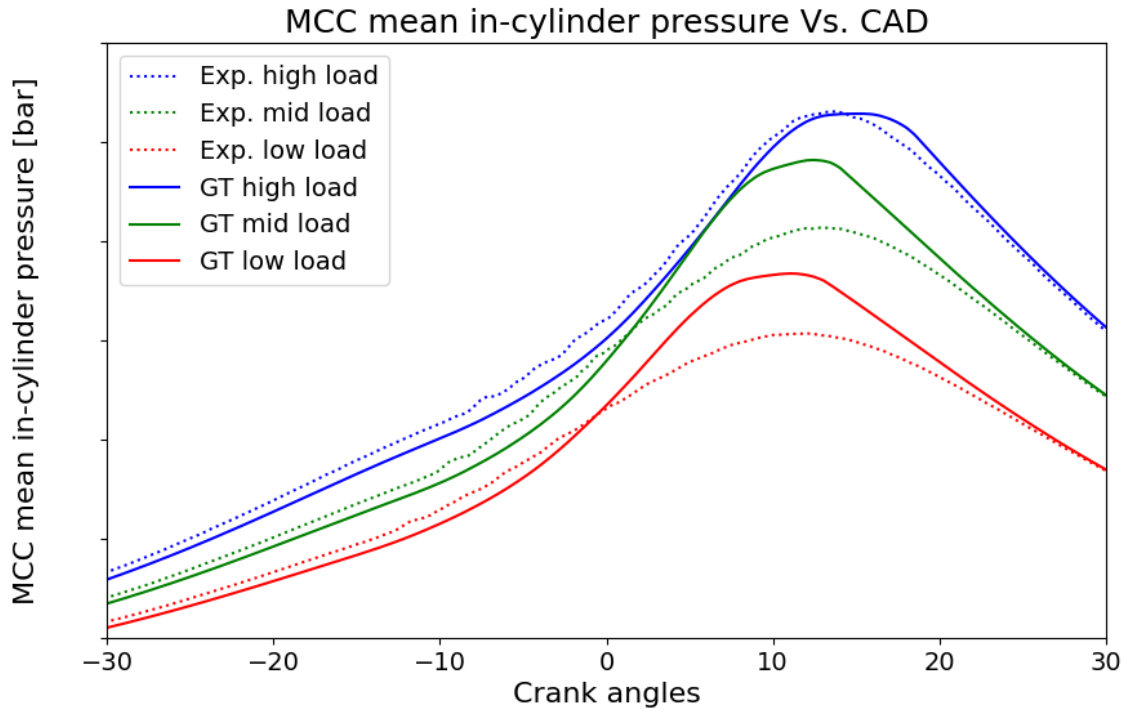

Figure 15. MCC in cylinder pressure with crank angles

Figure 15 depicts the in-cylinder pressure trace of MCC within the CAs to perform MCC HRR analysis. It can be seen from the graph that the colour combination remains the almost same as the PCC in-cylinder pressure trace in MCC in-cylinder pressure with fewer discrepancies for the high-load operation. Moreover, it can be noticed from the figure that based on the obtained experimental MCC pressure trace, the simulated model predicted the pressure data by similarly employing the TPA formula which shows that the data is ideally with slightly lower values before the TDC.

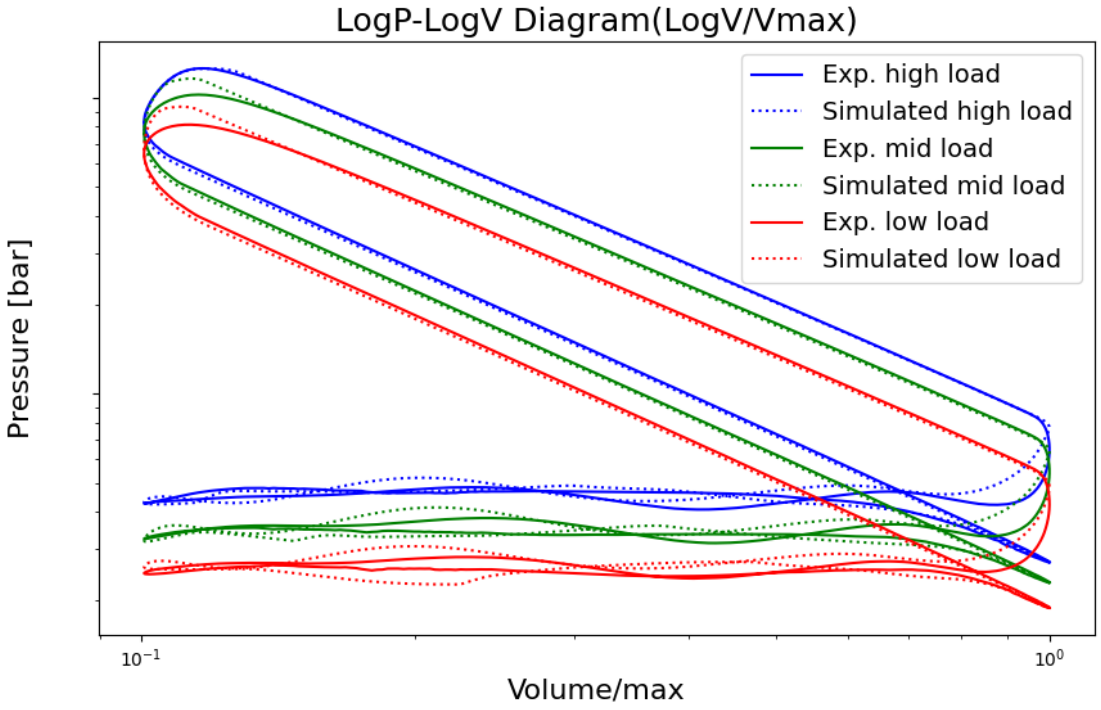

Figure 16. LogP-LogV diagram of MCC

Figure 16 demonstrates the logarithm of pressure against the volume of MCC that reveal the combustion behaviour of the engine cycle in each operating phase. It is employed to check the characteristics of the gas exchange loop of the cylinder pressure. The overall comparison of the experimental data points and the GT-model data is satisfactory throughout the engine cycle for these three operating points. Moreover, the compression and expansion phases reveal that the GT model's predictions are consistent

with experimental results in high-load, mid-load, and low-load, with only a few exceptions specifically within the mid and low load. The observed tuning is satisfactory, as the log P vs. log V plot magnifies fluctuations at lower pressure ranges, indicating no significant issues with the GT model tuning except fewer differences within the mid and low load.

The studied method analyses multiple PCC & MCC parameters, which include mean in-cylinder temperature, specific heat capacity ratio, heat transfer rate, air-fuel ratio (λ), gross HRR, and cumulative HRR of the developed model. These parameters have been compared against the simulated GT power results.

5.2 Validation of the developed HRR algorithm – pre-chamber results

The section entails the PCC outcomes of the high-load, mid-load, and low-load operations in the Python-developed HRR algorithm of different parameters. It validates these individual parameters against the simulated GT result. This consists of six different parameters of the PCC starting with mean in-cylinder gas temperature, specific heat capacity, heat transfer rate, HRR, cumulative HRR, and lambda at spark timing which have been validated using graphical comparison and then determined the error using MAPE method to ensure the discrepancies

5.2.1 PCC mean in-cylinder gas temperature

Figure 17 demonstrates the mean in-cylinder temperature among the calibrated GT-Power results and the Python-developed model of the three operating points. The graph depicts the high-load, mid-load, and low-load data of the mean in-cylinder gas temperature. The extracted results (solid blue, green, and red lines) from the simulated GT-Power model depict the characteristics of a single cycle while the dotted lines indicated the Python developed results. The colour combination remains stable for the other results validations.

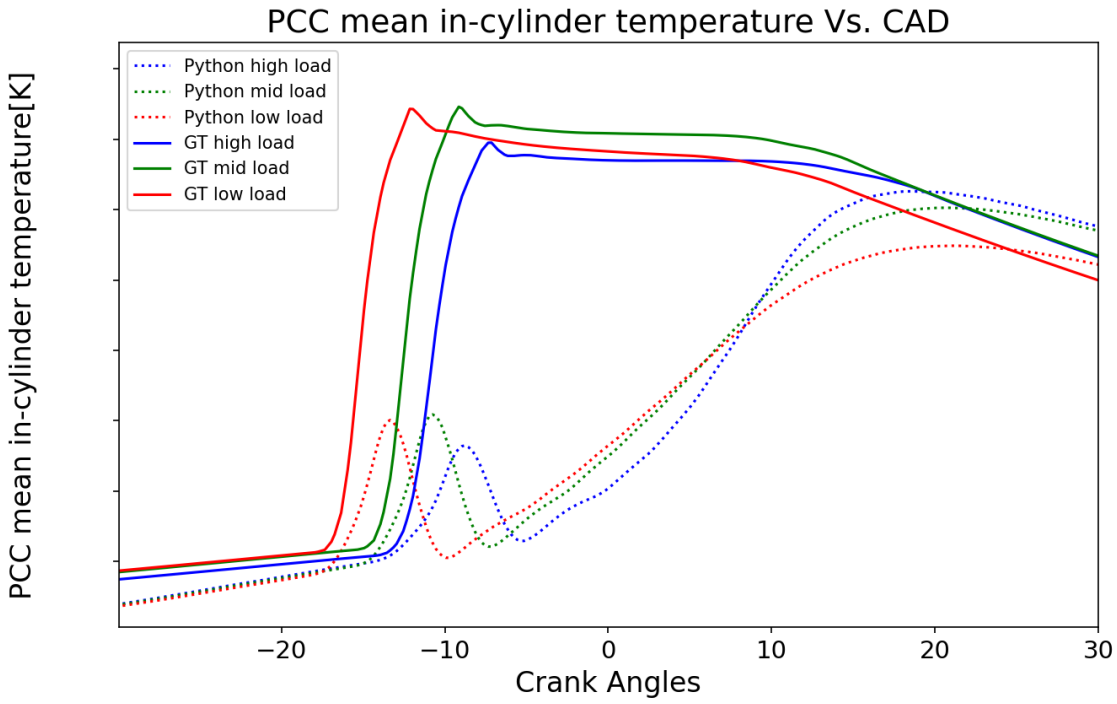

Figure 17. PCC mean in-cylinder gas temperature validation with crank angle

Although calibrated results reveal a higher culmination at temperatures with a rapid shift specifically close to the top dead centre (TDC) in all three operating points, the Python model uses ideal gas assumption to estimate gas temperature. The ideal gas assumption becomes weaker during the PCC combustion process due to intense mass transfer (considering a small volume of PCC). Due to this reason, the comparison was made only before the combustion for both the mean gas temperature of the simulated one and the developed model. The Python model load operations show a smoother decline in peaks while the GT result also reveals steady state data output. Additionally, the compression and expansion stages of combustion provide a solid correlation between the developed models and the calibrated GT-Power data outputs.

5.2.2 PCC specific heat capacity ratio

The comparison and validation of the PCC-specific heat capacity ratio tracing have been conducted using temperature and crank angle-based gamma tracing Equation (32). The

temperature and CA have been estimated based on the initial gamma calculation using NASA polynomial coefficients.

According to the line graph (Figure 18) the peak PCC heat capacity ratio of the averaged 300-cycle examined model is slightly lower than the calibrated GT-power model. The high load operation is closer to the calibrated GT results in comparison to the mid and low loads respectively. The combustion phase for specific heat capacity ratio estimation is windowed by considering the start of the combustion and the second pressure difference reversal which emphasizes on crucial phase where the gas properties predominantly affect the combustion phenomena.

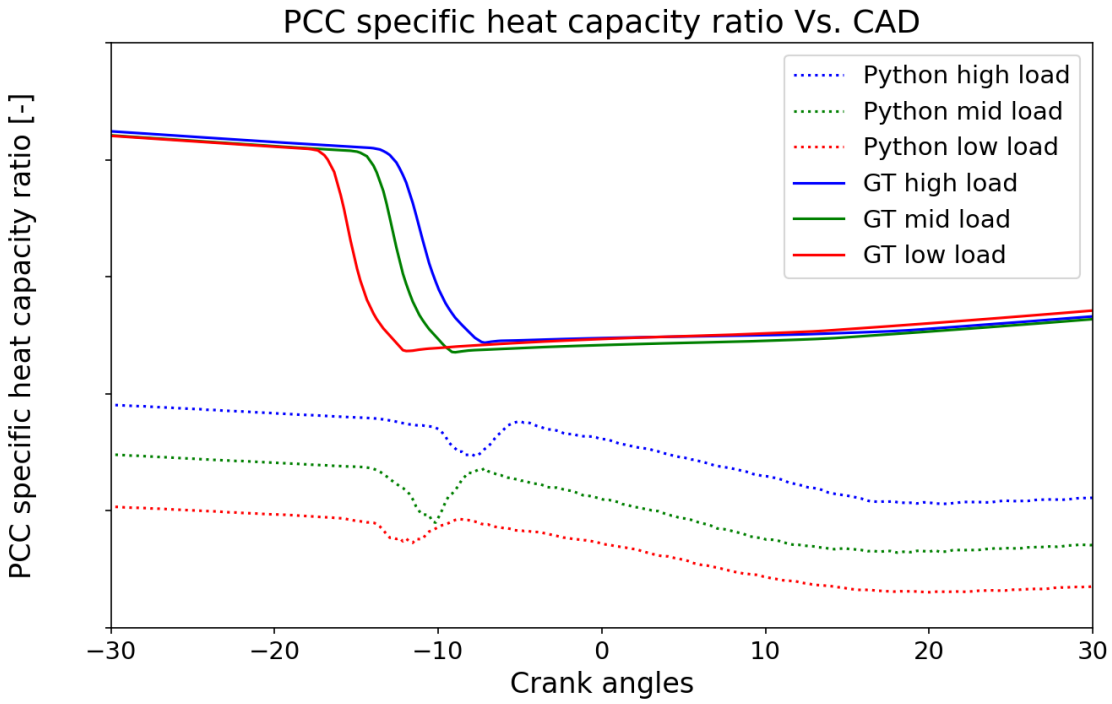

Figure 18. PCC specific heat capacity ratio with crank angles

The averaged data for Python-developed models experienced a decrease shortly before the end of the compression stroke and the start of the combustion, followed by a gradual increase in its peak value in all three cases. These increases maintained the stability of the specific heat capacity for PCC during the same stroke. Regarding the calibration

results, they abruptly decreased at the same point as the averaged results and remained stable till the end.

5.2.3 PCC heat transfer rate

Figure 19 presents a comparison between the PCC heat transfer rate from the Python-developed model and the simulated GT-Power data.

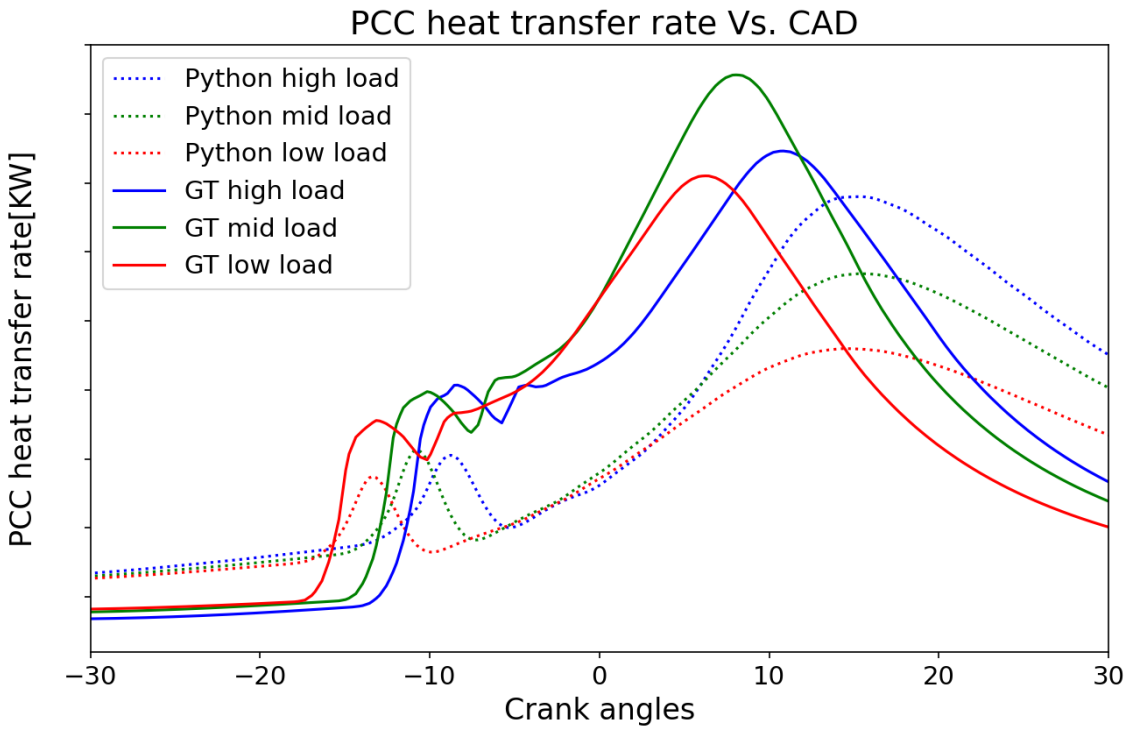

Figure 19. PCC heat transfer rate with crank angles

We have estimated the PCC heat transfer rate of the analyzed model using Equation (33). The graph reveals that the averaged data outputs of the Python-developed model in all three loads rise slightly with a peak close to the end of the compression stroke and then follow through a progressive rise until its highest level during the beginning of the expansion stroke, afterward a gradual reduction during the expansion stroke. In the case of the simulated results, which starts with a rapid increase at the end of the compression stroke with a spike after certain CAD from there, then a gradual climb until the highest

heat transfer rate and decline slowly during the expansion stroke in all three loads. The GT-Power data is comparatively higher than the Python model's average data.

5.2.4 PCC gross heat release rate

The PCC gross HRR is shown in Figure 20 compared to the simulated GT-power single-cycle output and the developed HRR model results for 300 engine cycles. We estimated the results of the developed model using the PCC gross HRR equation (Equation 41), which considers the PCC pressure trace, PCC volume, PCC specific heat capacity ratio, PCC mass flow, and the mean in-cylinder temperature of PCC during IVC and EVO. Following this, the assessed mean PCC HRR experienced a swift increase on the graph, reaching its peak point in all three cases. Meanwhile, the predicted GT-power output

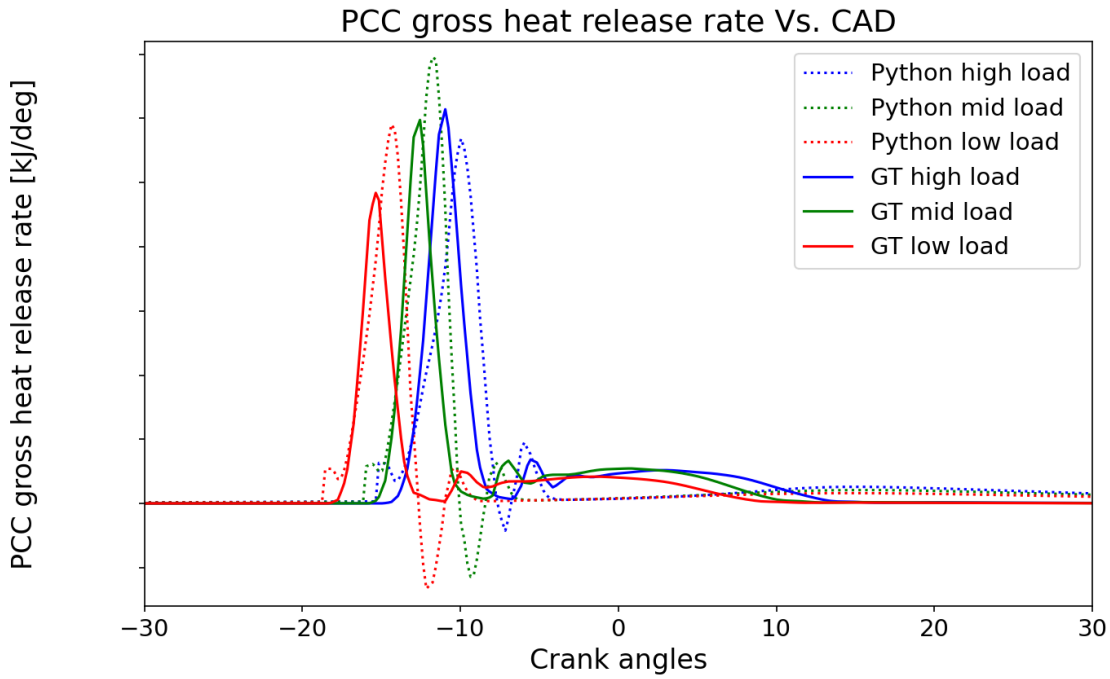

Figure 20. PCC gross heat release rate with crank angles

experienced a rapid growth in the HRR, reaching its highest level. The Python-developed model and GT-Power both quickly dropped after their highest point during combustion, but there were fewer positive and negative changes until the end. The high-load Python-

developed model, on the other hand, fell faster at around -9 CAD at the end of the compression stroke and then quickly rose until it reached a stable state around -7 CAD in the same stroke and similarly within the mid and low loads start slightly earlier than the high-load continue within the similar range for mid and low loads respectively. The PCC HRR has been windowing starting from the ignition to the second pressure difference reversal point which is around -6.35 CAD for capturing rapid changes in pressure and HRR.

5.2.5 PCC cumulative heat release rate

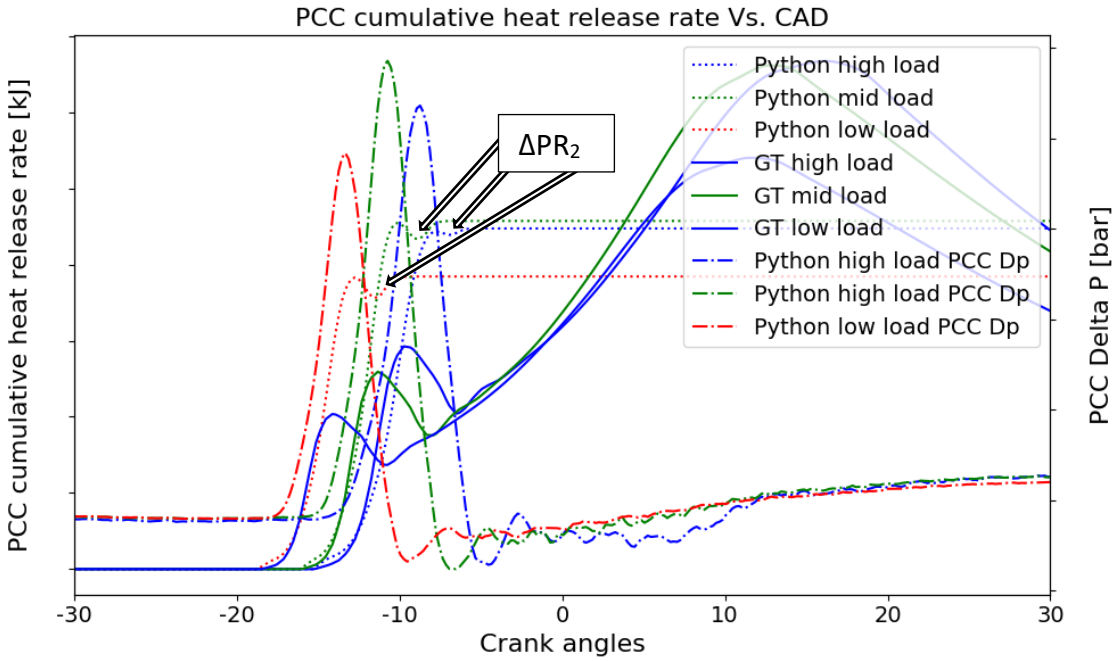

Figure 21. PCC cumulative HRR with crank angles.

Figure 21 shows the cumulative HRR of GT-power simulation results and the Python HRR model results. The variation in cumulative HRR against the CADs has been provided in the graph for three different operating points. To understand the widowing of the cumulative HRR the pressure difference between PCC and MCC ($\Delta P_{PCC\text{-}MCC}$) has also been plotted in this graph and referred to as (dashed-dotted) lines. The average PCC cumulative HRR from the studied model saw an instantaneous growth rate at around -15 CADs just before the end of the compression stroke in all three cases, and the Python data reached

the peak value and continued to be a flatline due to considering the windowed cumulative HRR until the second PCC pressure differences reversal point at -6.35 CAD after TDC within all operating data points. However, the simulated data appeared to have slight fluctuations just after its highest value until the end. Similar to the Python model, we considered the maximum value of the first peak. Moreover, disregarding the values after the peak value of GT decreases the fluctuation, providing a steadier comparison.

5.2.6 PCC lambda at spark timing

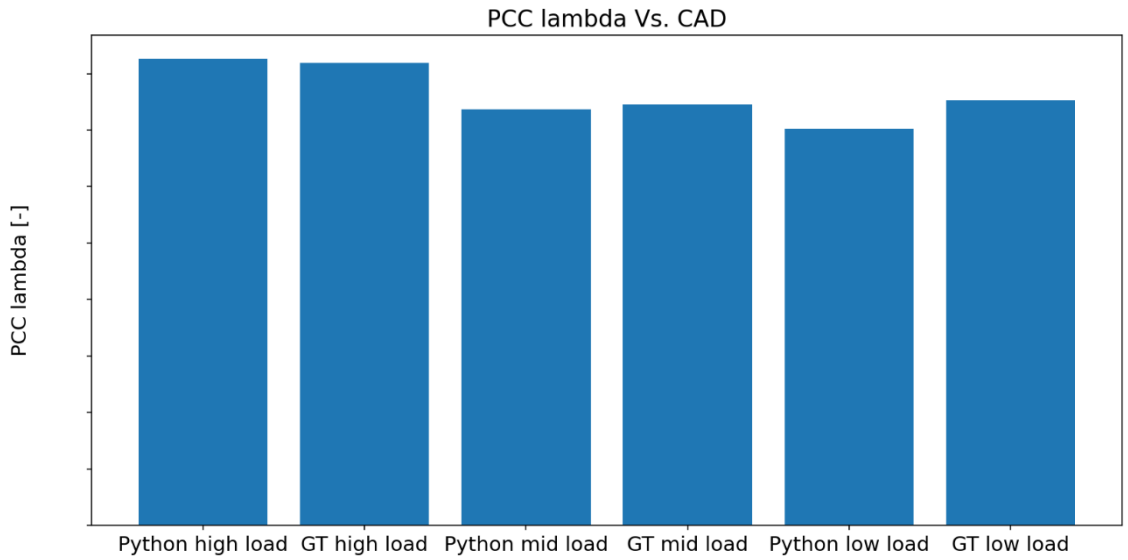

Figure 22. PCC lambda validation

The bar chart (Figure 22) provides the trace of lambda estimation at spark timing of both GT-power and Python developed PCC HRR model. It is observed from the result of high-load operation shows that the Python result captured almost similar output as the GT results. Similar phenomena have been experienced for the mid load operations as well, while in low load operation shows very little amount of differences withing the simulated results.

5.3 Validation of the developed HRR algorithm – main chamber results

Similar to the PCC results this subsection of the chapter validates the Python-developed MCC HRR algorithm by making the comparison with the GT simulation results including parameters similar to PCC considering the high, mid, and low load operations.

5.3.1 MCC mean in-cylinder gas temperature

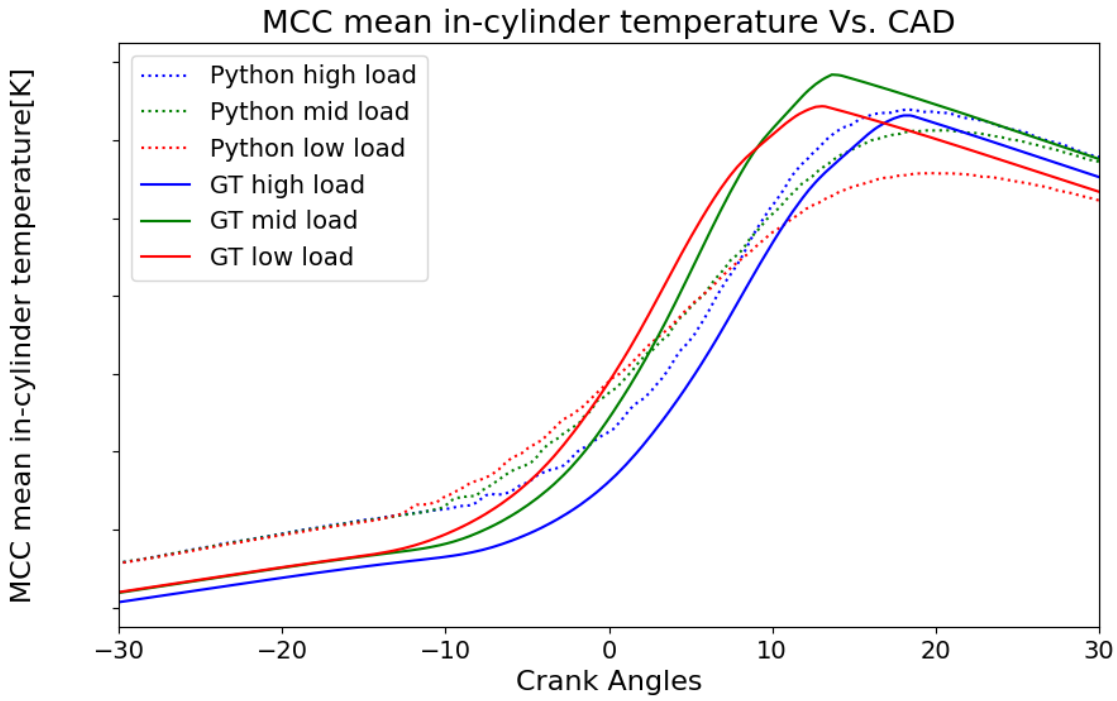

Figure 23. MCC mean in-cylinder temperature against crank angles

The line graph (Figure 23) compares the MCC mean in-cylinder temperature of both the calibrated GT-power result and the developed code results of three load operations. Moreover, the output has been depicted based on Equation 31, the mean gas temperature equation. The simulated model grew steadily during the compression phase, experienced a rapid increase just before the TDC, and then experienced a gradual decline during the expansion stroke in all three loads (high, mid, and low), although Python models mid and low load show more differences in comparison with high load against the simulated results. The analysed data indicates a similar start, albeit at slightly higher

temperatures than the GT-power data during the compression stroke. Figure 22 shows that after the averaged 300-cycle value, the curve quickly rose, especially just before the TDC and matching the simulated peak point at around 15 CAD after TDC in all three cases. This was followed by a steeper progressive decline in the expansion stroke than the GT model. Although there are slight discrepancies among both models specifically within the mid and low load, overall, the graph captured the broader range of the engine behaviour in both cases and met the desired output.

5.3.2 MCC specific heat capacity ratio

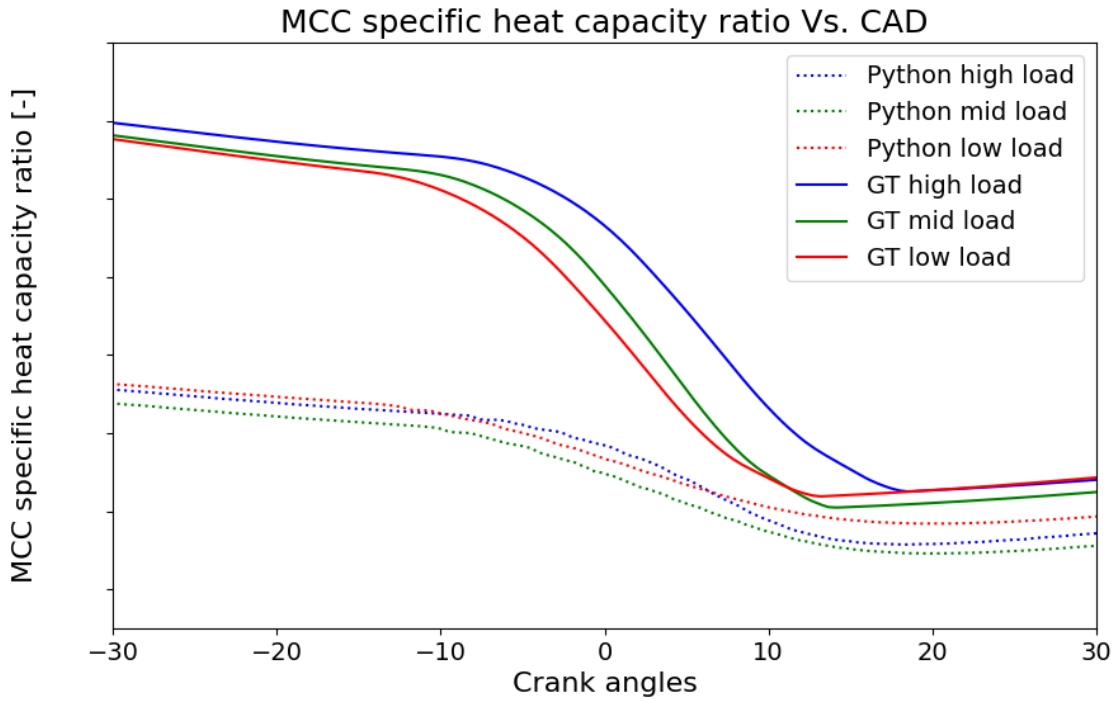

Figure 24. MCC specific heat capacity ratio

The line graph (Figure 24) provides the MCC specific heat capacity ratio trace of calibrated GT-power data and a Python model. The temperature and CA based gamma trace equation for MCC was employed to achieve this result (Equation 32). The mean gas temperature and the initial gamma are used to estimate the equation of MCC specific heat capacity ratio. The GT-power output in all three operations here indicates the ratio be-

fore the end of the compression phase. As per the simulated data, the specific heat capacity ratio of MCC experiences a sudden decrease after TDC, until the start of the expansion phase, which follows through a gradual growth during the expansion stroke.

However, the three operating loads (high, mid, and low) Python-analysed data results show that the specific heat capacity ratio is comparatively lower close to the end of the compression stroke than the simulated model. The Python data output also observes a slight decline at the end of the compression, followed by a steady fall until around, and then follows a slight growth till the end with very few differences in all three cases.

5.3.3 MCC heat transfer rate

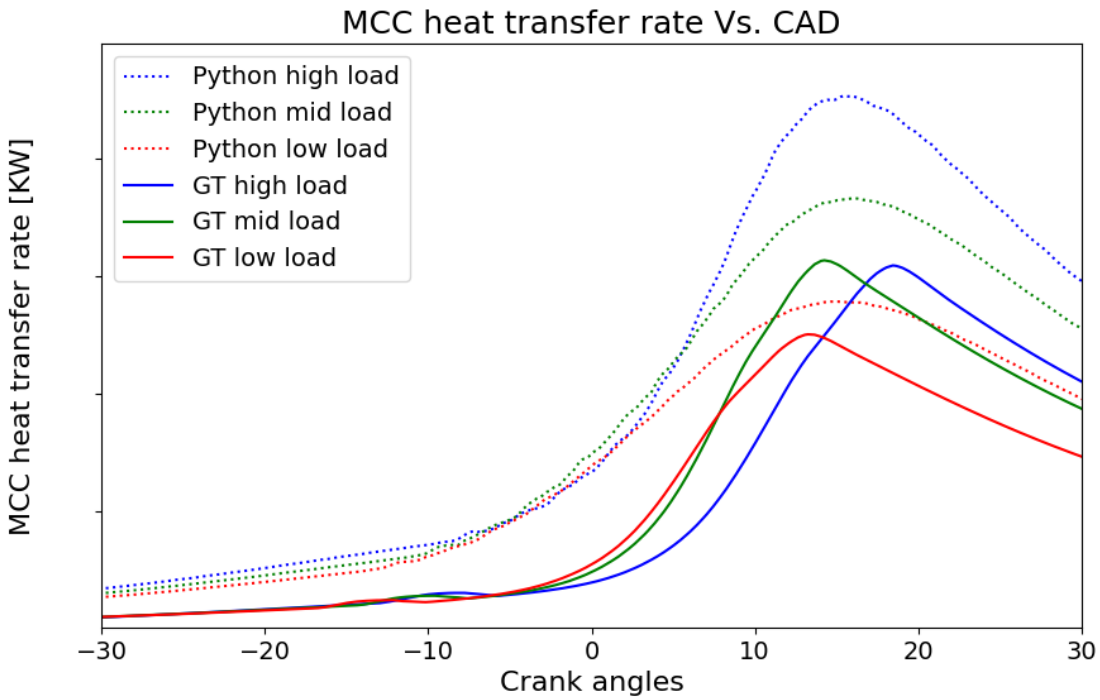

Figure 25. MCC heat transfer rate with crank angles

Figure 25 below illustrates the MCC heat transfer rate of GT-power results and Python data from the implemented model. We calculated the Python model output using the Woschni heat transfer rate calculation formula, which considers the MCC gas velocity

and motored pressure. Moreover, this led to estimates of the MCC convective heat transfer coefficient, which determines the overall MCC heat transfer rate. However, the Woschni model in Python code and GT are not exactly the same. The GT model uses Woschni-GT, with different coefficient values employed by the Python-developed model. According to the graph, the averaged Python model result has a higher MCC heat transfer rate during the combustion phase compared to the simulated model in GT-Power. The Python-developed operating points appeared to be slightly higher than the extracted GT output. The Python data's highest peak has some discrepancies within the GT results in high, mid, and low load operations. The reason behind the discrepancy is the method of estimating the heat loss is different as it considers different coefficient values, as mentioned earlier in this paragraph, which is why the graphs appear to have such differences.

5.3.4 MCC gross heat release rate

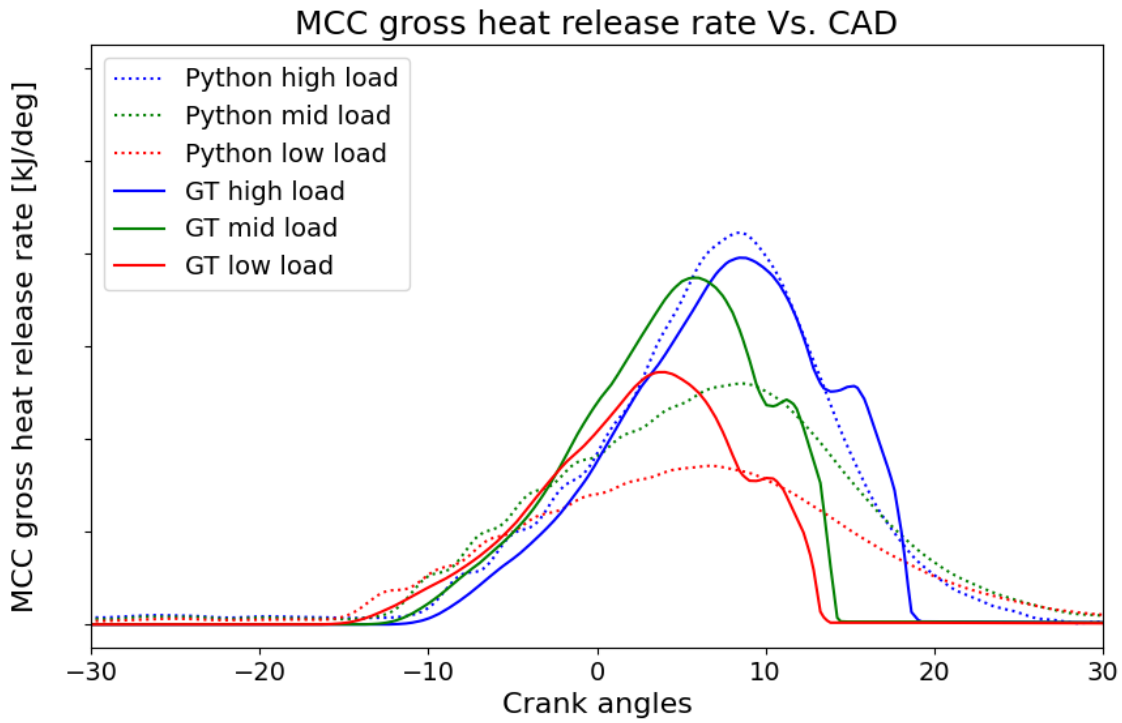

Figure 26. MCC gross heat release rate with crank angles

The gross HRR for the MCC has been estimated using the Equation (41) which was dependent on MCC specific heat capacity ratio. The Figure 26 illustrates the comparison and validation of the MCC gross HRR between the Python developed model and the GT-power simulated results. The three loads of Python model MCC HRR begin to increase slightly earlier than the GT-power data at the start of the combustion process. This continues until the GT-power results exceed the Python data at the peak point, just after the start of the expansion stroke whereas the simulated model reaches the highest point. The high load operations capture the similar phenomena of GT while the mid and low load operation shows slight discrepancies. Following a certain increase in both the output and the simulated results, there was a swift decline in the MCC HRR. Overall, the graph indicates a similar HRR phenomenon with fewer differences at mid and low load.

5.3.5 MCC cumulative heat release rate

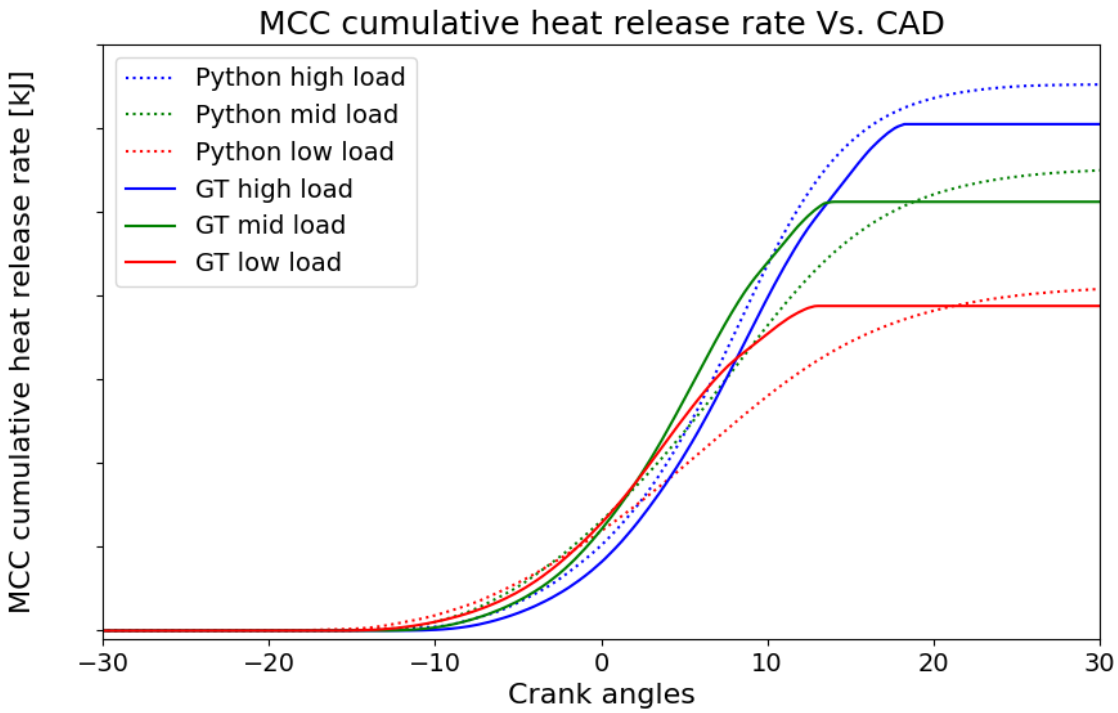

Figure 27. MCC cumulative heat release rate with crank angles

Figure 27 illustrates the cumulative HRR in the MCC, comparing the calibrated output of the HRR against the Python-developed results of three operating loads. For this combustion phase, windowing has been considered from the start of the ignition to the CA90 after TDC, at which the heat is released. Both Python MCC cumulative HRRs and the calibrated ones experienced a rapid increase in cumulative HRR, peaking closely to one another, respectively, just before the end of the compression phase and the start of the expansion phase and then stabilizing during the expansion stroke in all three loads with fewer differences.

5.3.6 MCC lambda at spark timing

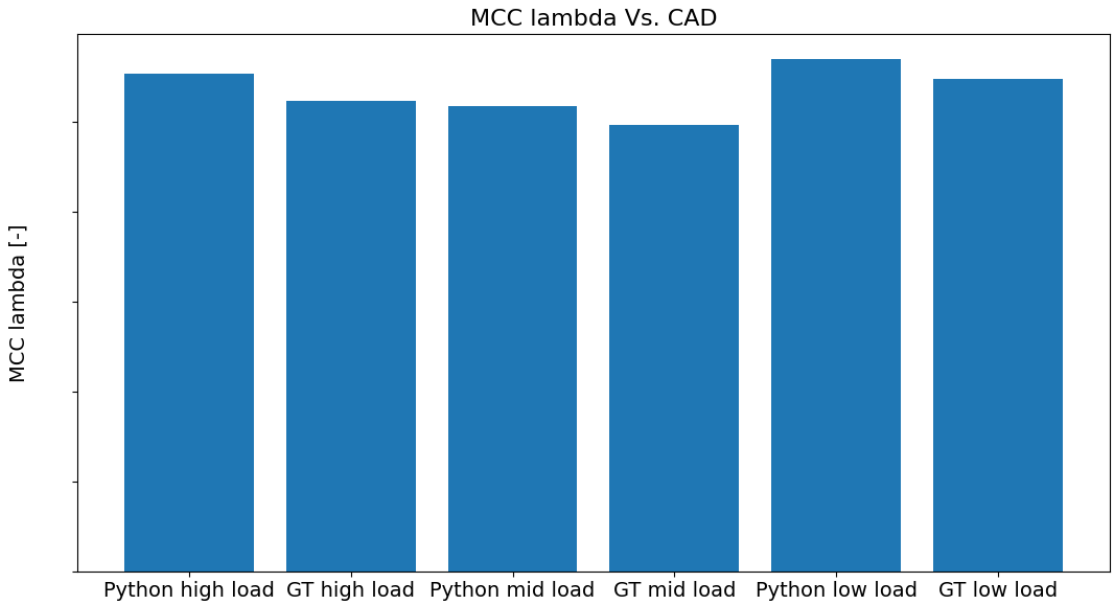

Figure 28. MCC lambda validation at spark timing

The bar chart (Figure 28) compares the MCC lambda at spark timing estimation results from GT-Power experiments and the model generated by this research work. The Python-developed lambda value of the high load and the calibrated lambda value are close to one another, respectively. Similarly, within Python-developed mid and low load operation experienced the similar outcome against the GT results. Furthermore, the graph indicates that the validation of the predicted model against the simulation results appears to be accurate, and the model is functioning correctly.

5.4 Validating interactions between PCC and MCC

Figure 29. indicates the interactions between MCC and PCC cumulative HRR of Python developed model against the simulated GT results. It is observed that the high load operation of the cumulative HRR of the Python model captured a comparatively closer trend of GT results. While mid and low-load results show slight differences against the GT results. The experimental pressure traces of the mid and low load had some differences with GT in comparison to the high load data which is another reason for such differences in the graph.

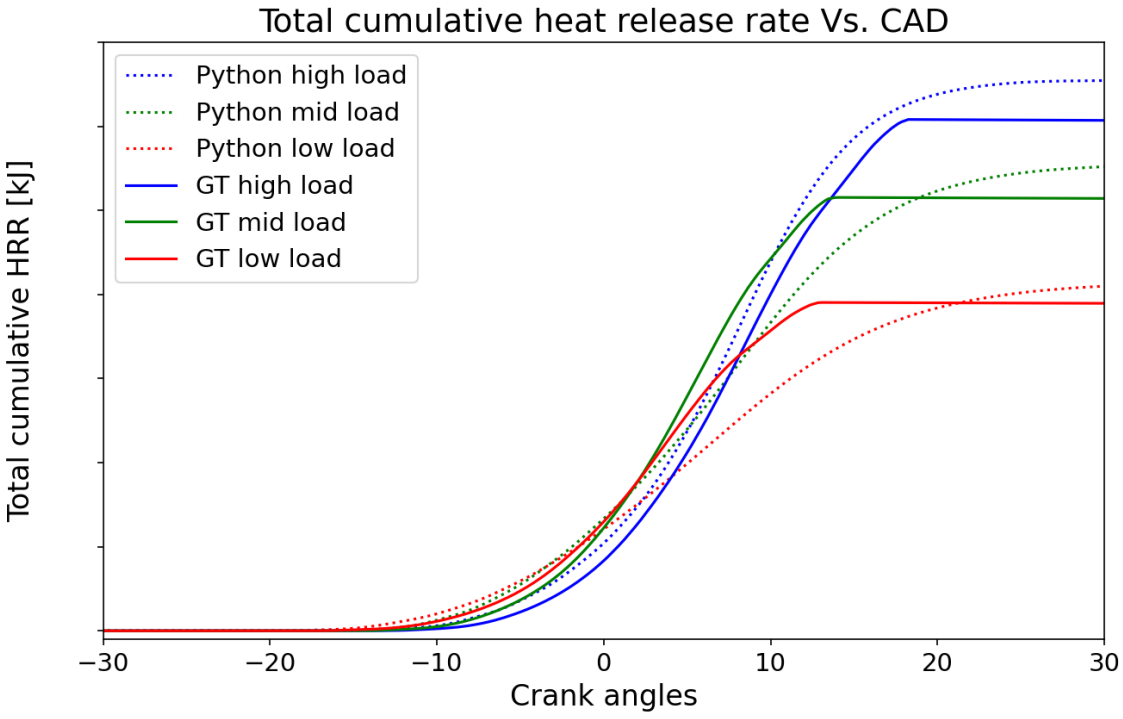

Figure 29. Total cumulative HRR against the CAD

5.5 HRR model performance across the operating points

The Python-developed HRR model validation has been conducted employing three operating points which are high, mid, and low loads from the referenced GT simulated data. The mean absolute error formula has been utilized for these operating points to ensure

the operating functionality and determine the accuracy of the model against the GT-Power results.

Table 2. Validated HRR model performance across the operating points

Discrepancies of HRR model parameters	**High-load MAPE**	**Mid-load MAPE**	**Low-load MAPE**
PCC mean in-cylinder temperature	6.3%	0.9%	12%
PCC specific heat capacity ratio	6.1%	0.5%	0.9%
PCC heat transfer rate	56%	50%	52%
PCC gross HRR	64%	66%	64%
PCC cumulative HRR	35%	61%	70%
PCC lambda at spark timing	0.09%	0.1%	0.3%
MCC mean in-cylinder temperature	9.3%	0.9%	10%
MCC specific heat capacity ratio	3.4%	0.3%	0.2%
MCC heat transfer rate	58%	46%	42%
MCC gross HRR	14%	39%	43%
MCC cumulative HRR	9.2%	11%	14%
MCC lambda at spark timing	5.6%	0.4%	0.3%

Table 2 reveals the mean absolute error of the three operating points considering the discussed Python-developed HRR model parameters earlier in this chapter. Starting with the PCC mean in-cylinder temperature, the table shows error percentage for high, mid, and low loads is 6.3%, 0.9%, and 12% respectively. Considering the ideal gas assumptions only before the combustion it becomes weaker in PCC due to intense mass. The mid-load point shows greater accuracy while the other two where the high load error proportion is half of the low load. Although assuming the gas before combustion leads to an acceptable outcome, the mean gas temperature estimation method can be further improved.

Secondly, table 2 validates the error percentage of the PCC-specific heat capacity ratio against the calibrated model using the MAPE. The table shows that the average PCC-

specific heat capacity ratio is 6.1%, 0.5%, and 0.9% MAPE. The observation points out that the studied model estimates the specific heat capacity accurately. The error percentage indicates that it is in the considerable range. However, there is still scope for further improvement.

Next, table 2 indicates that the PCC heat transfer rate error percentage based on the MAPEs are relatively high in the percentage (56%, 50%, and 52%) in high, mid, and low loads data points of the Python model against the GT-power results. The main reason for the differences within the PCC heat transfer rate is that the calculations of the GT and developed models are different. The simulated GT model used the flow method to estimate the heat transfer model, while the Python-developed model employed the Woschni formula. Along with that, the Woschni heat transfer model is effective for the MCC of ICE. However, PCC has highly turbulent flow and complex geometries that were not considered in the Woschni model, and this leads to error since it does not capture intense turbulent flows and complex geometries of the PCC. This enables further research and development of heat transfer rate models for PCC engines.

Afterwards, table 2 provides the error percentage in MAPE for the gross PCC HRR model is high for all three data points which are 64%, 66%, and 64%. The reasons behind this error in PCC gross HRR starting with the PCC mean gas temperature which shows a higher discrepancy within traces against the GT results. Along with that, the simulated model couldn’t completely capture the experimental PCC pressure traces in all three operating points which is why these are leading to error percentage in the validation to some extent. Since this validation model shows some discrepancies, further research can be conducted to improve the model by enhancing the mean gas temperature.

Then, table 2 indicates the PCC cumulative HRR validation against the simulated results using MAPE for three operating loads which are around 35%, 61%, and 70%. Windowing the PCC phase ranging from the start of ignition to the second reversal point CAD before TDC provides larger insights into the PCC combustion process.

As the cumulative HRR depends on the PCC HRR, the error percentage here is also high as expected. Because of the mean gas temperature error of the PCC model causing such error and the close look observance of the small geometry leading to a higher error percentage, however, this model can be further improved by mitigating the errors and providing reliable cumulative HRR.

To validate PCC lambda estimation, we have employed MAPE as shown in Table 2. For validation, we consider only a single point value starting with before the start of combustion. The reason for this is that the fuel injection into PCC is not appropriately modelled here in GT. The error percentage between the average PCC lambda for high, mid, and low loads are 0.09%, 0.1%, and 0.3% against the GT-power model. Although the error percentage is much less, the calibration of the reference model requires adjustments and improvements that can be performed in future research.

As per table 2, the validation of the MCC means in-cylinder temperature has been conducted by employing the MAPE which shows the difference between the Python data and the simulated data where the mean value for high, mid, and low loads are 9.3%, 0.9%, and 10%. This implies that the validation of this calculation is reasonably accurate.

Table 2 also shows the MCC heat capacity ratio discrepancy between the GT-power model and the Python-developed model results validated using MAPE. It is seen from the table that the model is validating reasonably accurate estimation considering the mean value for the three points are only 3.4%, 0.3%, and 0.2% errors. It is clear from the validation that the model is accurate and can be further improved as well.

For validation of the MCC heat transfer model windowing the combustion phase from the start of the combustion to around CA90 after TDC to capture the crucial heat transfer phenomenon. Table 2 reveals that the average MCC heat transfer rate showed around 58%, 46%, and 42% error for three different loads. The method of estimating the heat transfer rate coefficient value is different in the Python model and then in the GT which

leads to such errors. The MAPE validation indicates that the model can be further improved by adjusting the coefficients and opening up the scope of future research.

It can be seen from table 2 that the average MCC gross HRR shows only 14%, 39%, and 43% differences within the simulated model. Moreover, the average discrepancy suggests that the validation is estimating considerably accurate value within the high load. However, the mid and low load shows quite high errors as per the MCC pressure GT could not completely capture the experimental pressure traces resulting in such errors in these values.

Table 2 also reveals the validation of the studied MCC cumulative HRR against the simulated GT-power results employing the MAPE formula. The MAPE for the average cumulative HRR for three operating points is 9.2%, 11%, and 14%. The comparison and the validation overall seem reasonably accurate for cumulative HRR.

Lastly, table 2 shows the MCC lambda value of the Python-developed model with the simulated data output. The MCC lambda validation considers from the bottom dead centre (BDC) ranging from (-180 CAD) to the start of ignition for capturing the lambda values. It can be observed that the error percentage of the MCC lambda for the three loads is 5.6%, 0.4%, and 0.3% in average error percentage. The validation of the MCC lambda shows the estimation is accurate.

Overall, it can be observed that the developed Python model is showing reasonable outcomes with fewer exceptions within all three operating points. Specifically, the PCC mean gas temperature affects the PCC gross HRR results. Moreover, the PCC heat transfer method can be further improved and for the MCC adjusting the coefficients will allow for improving the errors.

5.6 Discussion

The validation and comparison of the PCC and MCC HRR models demonstrate the strengths and limitations of estimating combustion characteristics considering three different operating points. Starting with the PCC, the mean in-cylinder temperature considering ideal gas assumption and making comparisons only before combustion provides significant results with considerable error percentage in validation. The PCC heat capacity ratio was also shown promising comparison and considerable error percentage. Due to the usage of the Woschni formula in heat transfer calculations, which does not capture the turbulence in PCC, there is inaccuracy in heat losses. With regards to PCC HRR, although the model shows the difference is quite small, the amount of error percentages in all three loads showing in the validation is due to the mean gas temperature error leading to such error percentage in PCC HRR validation. Moreover, the cumulative HRR and the PCC lambda estimation provide comparatively better predictions than PCC HRR and heat transfer rates.

In the MCC HRR model, most of the parameters considering all three loads (high, mid, and low) of this model show decent accuracy in predicting the model. The mean in-cylinder MCC temperature and the MCC-specific heat capacity ratio provide good accuracy with low error in the validation. Additionally, the MCC HRR and cumulative HRR outline adequate precision in estimating the HRR model. However, the MCC heat transfer rate shows a high error percentage in the validation while the MCC lambda estimated significant results with a fraction of errors in the validation.

The Python-developed HRR model tool has been implemented mainly for usage as a comparison between different operating conditions. Therefore, based on the validation and estimations, it can be observed the phenomenological HRR model is capturing vital combustion phenomena, peak HRR, and overall combustion as a whole operating accu-

rately under certain conditions. However, fewer discrepancies in the PCC validation compared to GT results show areas for further improvement. Thus, the implemented HRR tool can be employed in engine performance analysis and optimization with up-and-coming refinement and modifications to work on different operating conditions.

6 Conclusions

This research work aimed at developing phenomenological HRR analysis model for PCC and MCC for SCE using open-source Python programming language. The research investigation is consisting of three prime objectives, depending on the results, comparison and validation these are outlined in the following part of this chapter.

1. This thesis successfully developed a phenomenological HRR model for multi-chamber SCE. The model has been developed in Python open-source programming platform. The operating time for the three different loads is less than 90 seconds. The difference in operating time between each load is not more than 2-3 seconds. This fast operation makes it suitable for Wärtsilä W31 SG SCE. The simplified phenomenological HRR model are open source which implies that the model allows for reduced the computational time and expenses while the thorough GT-Power models are highly time consuming and expensive with GT-suite licensing.
2. The Python-developed model has considered three different operating loads which are high, medium, and low loads of the W31 SG SCE, and it is observed that for each case, the mean absolute error shows reasonable accuracy in estimation with fewer exceptions in certain parameters. This model considered the gross HRR, heat losses, instantaneous gamma, cumulative HRR, mean gas temperature, and lambda values at spark timing for both the PCC and MCC. Although the PCC mean gas temperature, gross HRR, and MCC and PCC heat losses show some discrepancies, other parameters show reasonable estimation results.
3. In this study, the total three operating loads from three pressure analysis model (TPA) implemented in GT-Suite Software is considered where the proposed Python model has been validated for all three cases to ensure the consistency of the model. To ensure the referenced GT models tuning it has been calibrated against the experimental pressure traces from the W31 SG SCE. The developed Python model employed the MAPE formula for determining the

error percentage which indicates the estimation accuracy and open up the scope for further research.

The research study successfully implemented a phenomenological HRR model for a PCC SCE that can potentially estimate the HRR with quick computation using Python open-source programming and has been validated against the referenced GT-Power results. The model has been constructed based on the experimental data and in-cylinder pressure traces, estimating the gross HRR employing the first law of thermodynamics while considering other parameters such as heat losses and heat capacities. This coming subsection of this chapter will sum up the thesis structure, concisely outlining the key outcomes of the research investigation and suggesting prospective future work.

6.1 Summary

The first chapter (Introduction) starts by introducing climate change and initiatives and then the roles of ICEs in the global economy, and its large-scale infrastructure, along with the ICE advancement, marine and powerplant solutions of ICE including introducing the lean burn phenomena of ICE allowing enhancement in efficiency. The next section of this chapter deals with PCC technologies describing the fundamentals and types of this technology. Following this, the phenomenological HRR models have been demonstrated, and the corresponding benefits of this approach have been pointed out.

Chapter 2, the problem statement chapter, outlines the corresponding problem and addresses the research question of the analysis asking for the novelty of the research, why it is required, and what has been done to develop this. Lastly, describe the architecture of the thesis.

Chapter 3 is the theoretical framework, which begins with the evolution of PCC technology from the 20th century to today. Moreover, pointing out the different concepts of PCC that have been introduced over the period, revealing the outcome of each model. The coming subsection demonstrates the core concepts of the PCSI system with detailed

understanding, types of it as well as the advantages and disadvantages of the PCC. Afterward, describing the thorough approach of phenomenological HRR and briefly introduce the HRR calculation approach.

Chapter 4 is the methodology which describes the object and the thorough approach for implementing the HRR model. The next subsection demonstrates the step-by-step process of the SCE multi-chamber HRR model. Based on the primary flowchart the following section covers the extracting of average PCC and MCC pressure data. Afterward, the chapter estimates the initial gamma, temperature, and crank angle-based gamma tracing for PCC and MCC. Furthermore, the PCC and MCC mean in-cylinder temperature and mass calculation. Then, estimating the convective heat transfer coefficient leads to calculating the heat transfer rate. After that, the model applies the first law of thermodynamics to estimate the gross HRR for PCC and MCC. However, the PCC also considers the PCC mass transfer rate and the enthalpy mass transfer rate in PCC due to mass exchange between the PCC and MCC, determining the gross HRR in the PCC. Moreover, it also provides an understanding of windowing the combustion phase. Next, it describes the fundamental understanding of the referenced GT model and outlines calculation methods. Lastly, the code structure subsection demonstrates the different subscripts of the code and the working principles of the code.

Chapter 5 which is the result and discussion demonstrates the implementation and results of the methodology. Firstly, it introduces the referenced GT results, including the differences and the method of comparing and validating the data with the developed model. The MCC & PCC in-cylinder pressure traces and experimental logarithm pressure-volume (LogP-LogV) trace with the simulated result to ensure calibration. Next, the chapter has two main subsections one is PCC comparison and validation, and the other one is the MCC. It reveals each of the crucial parameter results that are derived in Chapter 4. For instance, illustrating the comparison of PCC & MCC in-cylinder gas temperature and validating these outcomes. Likewise, for the temperature and crank-angle-based gamma

tracing, lambda value as well as the heat transfer rate has been compared with the simulated GT results and validated using the MAPE method. Furthermore, the gross HRR and the cumulative HRR of PCC and MCC were compared, and these observations were validated within the tuned GT results. Finally, discuss the results and validation of this chapter in the last subsection including the discrepancy.

Chapter 6 is the conclusion that begins by answering the research objectives and demonstrating the thesis work. Additionally, explaining the necessity of this development in engine research. Next, it summarizes the whole thesis and follows through on suggestions for prospective future work that opens up the scope for further development and refinement.

6.2 Future work

Although the implemented phenomenological HRR model for the SCE is operating successfully, there is always room for improvement and adjustment of the calibration parameters. Various areas can be considered in terms of improving the model, such as the mismatch of the PCC mean in-cylinder temperature calculations can be an opportunity to enhance the model further. Improvement of PCC heat transfer loss estimation methods will lead to demonstrating better results in comparison to the current outcomes. Moreover, integration of flow heat transfer model can be a potential option to work more on enhancing the heat losses accuracy. Also, the PCC heat capacity ratio can be further improved, and modified to perform more accurate estimation.

The inclusion of not only the SCE HRR model but also other engine types will broaden the capability of the HRR model. Furthermore, validation of HRR with the various kinds of engines, different operational conditions, and different empirical data will ensure the stability of the developed system.

Reference

A. Bagnulo. (1947). *Engine with Stratified Mixture* (Patent No. 2422610).

Aabo, K. (2020). *The role of combustion engines in decarbonization – seeking fuel solutions*. https://www.dnv.com/expert-story/maritime-impact/The-role-of-combustion-engines-in-de-carbonization-seeking-fuel-solutions/

Adams, Tim G. (1979, February). Torch Ignition for Combustion Control of Lean Mixtures. *1979 Automotive Engineering Congress and Exposition*. https://doi.org/10.4271/790440

Alvarez, C. E. C., Couto, G. E., Roso, V. R., Thiriet, A. B., & Valle, R. M. (2018). A review of prechamber ignition systems as lean combustion technology for SI engines. *Applied Thermal Engineering*, *128*, 107–120. https://doi.org/10.1016/j.applthermaleng.2017.08.118

Annand, W. J. D. (1963). Heat Transfer in the Cylinders of Reciprocating Internal Combustion Engines. *Proceedings of the Institution of Mechanical Engineers*, *177*(1), 973–996. https://doi.org/10.1243/PIME_PROC_1963_177_069_02

Attard, W. P., & Blaxill, H. (2012, April). A Lean Burn Gasoline Fueled Pre-Chamber Jet Ignition Combustion System Achieving High Efficiency and Low NOx at Part Load. *SAE 2012 World Congress & Exhibition*. https://doi.org/10.4271/2012-01-1146

Attard, William P. & Blaxill, Hugh. (2011). A Single Fuel Pre-Chamber Jet Ignition Powertrain Achieving High Load, High Efficiency and Near Zero NOx Emissions. *SAE International Journal of Engines*, *5*(3), 734–746. https://doi.org/10.4271/2011-01-2023

Attard, William P., Fraser, Neil, Parsons, Patrick, & Toulson, Elisa. (2010). A Turbulent Jet Ignition Pre-Chamber Combustion System for Large Fuel Economy Improvements in a Modern Vehicle Powertrain. *SAE International Journal of Engines*, *3*(2), 20–37. https://doi.org/10.4271/2010-01-1457

Balmelli, M., Rogers, D., Hilfiker, T., Wright, Y., & Soltic, P. (2024). Method for pressure trace based thermodynamic analysis of pre-chamber combustion. *Energy Conversion and Management*, *312*, 118561. https://doi.org/10.1016/j.enconman.2024.118561

Barba, C., Burkhardt, C., Boulouchos, K., & Bargende, M. (1999). An empirical model for precalculating the combustion rate of the Common Rail Diesel engine for passenger cars. *MTZ Motortechnische Zeitschirft*, *60*.

Barba, C., Burkhardt, C., Boulouchos, K., & Bargende, M. (2000). A phenomenological combustion model for heat release rate prediction in high-speed DI Diesel engines with common rail injection. *SAE Technical Paper*.

Brandstetter, W. (1980). The Volkswagen Lean Burn PC-Engine Concept. *SAE Transactions*, *89*, 1804–1821. JSTOR.

Brunt, M. F., Rai, H., & Emtage, A. L. (1998). The calculation of heat release energy from engine cylinder pressure data. *SAE Transactions*, 1596--1609.

Ceviz, M. A., & Kaymaz, İ. (2005). Temperature and air–fuel ratio dependent specific heat ratio functions for lean burned and unburned mixture. *Energy Conversion and Management*, *46*(15), 2387–2404. https://doi.org/10.1016/j.enconman.2004.12.009

Climate change mitigation: Reducing emissions. (2024). https://www.eea.europa.eu/en/topics/in-depth/climate-change-mitigation-reducing-emissions?activeAccordion=&activeTab=fa515f0c-9ab0-493c-b4cd-58a32dfaae0a

Cylinder Pressure Analysis—Gamma Technologies. (2023). Gamma Technologies. https://www.gtisoft.com/cylinder-pressure-analysis/

Date, T., Yagi, S., Ishizuya, A., & Fujii, I. (1974). Research and development of the Honda CVCC engine. *SAE Transactions Paper*.

Dober, G. (1999). Modelling the flame enhancement of a HAJI equipped spark ignition engine. *SAE No.99091*. https://cir.nii.ac.jp/crid/1570854174262060032

European Commission & Directorate-General for Climate Action. (2019). *Going climate-neutral by 2050 – A strategic long-term vision for a prosperous, modern, competitive and climate-neutral EU economy*. Publications Office. https://doi.org/doi/10.2834/02074

Gamma Technologies. (n.d.). *GT-Power*. Gamma Technologies. Retrieved October 10, 2024, from https://www.gtisoft.com/gt-power/

Garcia-Oliver, J., Niki, Y., Rajasegar, R., Novella, R., Gomez-Soriano, J., Martínez, P., Li, Z., & Musculus, M. (2021). An experimental and one-dimensional modeling analysis of turbulent gas ejection in pre-chamber engines. *Fuel*, *299*, 120861. https://doi.org/10.1016/j.fuel.2021.120861

Gatowski, J., Balles, E. N., Chun, K. M., Nelson, F., Ekchian, J., & Heywood, J. B. (1984). Heat release analysis of engine pressure data. *SAE Transactions*, 961--977.

Getzlaff, J., Pape, J., Gruenig, Kuhnert, D., & Latsch, R. (2007). Investigations on pre-chamber spark plug with pilot injection. *SAE Transactions*, 421--433.

Gussak, L. A., Karpov, V. P., Slutskii, V. G., & Spasski, A. I. (1983). Burning rate and stability in forechamber flame ignition in an internal-combustion engine. *Combust., Explos. Shock Waves (Engl. Transl.); (United States)*, *19:5*. https://doi.org/10.1007/BF00750441

Gussak, L. A., Turkish, Michael C., & Siegla, Donald C. (1975, February). High Chemical Activity of Incomplete Combustion Products and a Method of Prechamber Torch Ignition for Avalanche Activation of Combustion in Internal Combustion Engines. *SAE Automobile Engineering and Manufacturing Meeting*. https://doi.org/10.4271/750890

Heywood, J. B. (2018). *Internal Combustion Engine Fundamentals* (2nd Edition). McGraw-Hill Education. https://www.accessengineeringlibrary.com/content/book/9781260116106

Hlaing, P. (2022). *Influence of Internal Geometry on Pre-chamber Combustion Concept in a Lean Burn Natural Gas Engine* [Doctoral Thesis (compilation)].

Hohenberg, G. F. (1979, February). Advanced Approaches for Heat Transfer Calculations. *1979 SAE International Off-Highway and Powerplant Congress and Exposition*. https://doi.org/10.4271/790825

Kalghatgi, G., Agarwal, A. K., Senecal, K., & Leach, F. (2022). Introduction to Engines and Fuels for Future Transport. *Engines and Fuels for Future Transport*, 1--5.

Kalghatgi, G. T. (2015). Developments in internal combustion engines and implications for combustion science and future transport fuels. *Proceedings of the Combustion Institute*, *35*(1), 101–115. https://doi.org/10.1016/j.proci.2014.10.002

Kawabata, Yasuharu & Mori, Daichi. (2004, March). Combustion Diagnostics & Improvement of a Pre-chamber Lean-Burn Natural Gas Engine. *SAE 2004 World Congress & Exhibition*. https://doi.org/10.4271/2004-01-0979

Leach, F., Kalghatgi, G., Stone, R., & Miles, P. (2020). The scope for improving the efficiency and environmental impact of internal combustion engines. *Transportation Engineering*, *1*, 100005. https://doi.org/10.1016/j.treng.2020.100005

Mallory, M. (1938). *Internal Combustion Engine* (Patent No. 2121920).

Noguchi, M., Sanda, S., & Nakamura, N. (1976, February). Development of Toyota Lean Burn Engine. *1976 Automobile Engineering Meeting*. https://doi.org/10.4271/760757

Novella, R., Morena, J. D. la, Pagano, V., & Pitarch, R. (2023). Optical evaluation of orifice orientation and number effects on active pre-chamber spark ignition combustion. *Fuel*, *338*, 127265. https://doi.org/10.1016/j.fuel.2022.127265

Oppenheim, A., Beltramo, J., Faris, D., & Maxson, J. (1989). Combustion by pulsed jet plumes-key to controlled combustion engines. *SAE Transactions*, 175--182.

Rajasegar, R., Niki, Y., Garcia-Oliver, J., Li, Z., & Musculus, M. (2021). Fundamental insights on ignition and combustion of natural gas in an active fueled pre-chamber spark-ignition system. *Combustion and Flame*, *232*. https://doi.org/10.1016/j.combustflame.2021.111561

Reitz, R. D., Ogawa, H., Payri, R., Fansler, T., Kokjohn, S., Moriyoshi, Y., Agarwal, A. K., Arcoumanis, D., Assanis, D., Bae, C., Boulouchos, K., Canakci, M., Curran, S., Denbratt, I., Gavaises, M., Guenthner, M., Hasse, C., Huang, Z., Ishiyama, T., … Zhao, H. (2020). IJER editorial: The future of the internal combustion engine. *International Journal of Engine Research*, *21*(1), 3–10. https://doi.org/10.1177/1468087419877990

Rezaei, R., Dinkelacker, F., Tilch, B., Delebinski, T., & Brauer, M. (2016). Phenomenological modeling of combustion and NOx emissions using detailed tabulated chemistry methods in diesel engines. *International Journal of Engine Research*, *17*(8), 846–856. https://doi.org/10.1177/1468087415619302

Ricardo, H. R. (1922). RECENT RESEARCH WORK ON THE INTERNAL-COMBUSTION ENGINE. *SAE Transactions*, *17*, 1–93. JSTOR.

Roethlisberger, R. P., & Favrat, D. (2002). Comparison between direct and indirect (prechamber) spark ignition in the case of a cogeneration natural gas engine, Part I: Engine geometrical parameters. *Applied Thermal Engineering*, *22*. https://doi.org/10.1016/S1359-4311(02)00040-6

Ryu, H., Chtsu, A., & Asanuma, T. (1987). Effect of Torch Jet Direction on Combustion and Performance of a Prechamber Spark-Ignition Engine. *SAE Transactions*, *96*, 201–211. JSTOR.

Sakai, Y., Kunii, K., Tsutsumi, S., & Nakagawa, Y. (1974). Combustion characteristics of the torch ignited engine. *SAE Transactions*, 3504--3512.

Sane, H., Purandare, N., Barve, O., & Todakar, A. (2014). Emission Reduction of IC engines by using water-in-diesel emulsion and catalytic converter. *International Journal of Research in Engineering and Technology*, *3*, 378--383.

Shah, A., Per, T., & Johansson, B. (2012). Investigation of Performance and Emission Characteristics of a Heavy Duty Natural Gas Engine Operated with Pre-Chamber Spark Plug and Dilution with Excess Air and EGR. *SAE International Journal of Engines*, *5*(4), 1790–1801. https://doi.org/10.4271/2012-01-1980

Silva, M., Sanal, S., Hlaing, P., Cenker, E., Johansson, B., & Im, H. (2020, April). *Effects of Geometry on Passive Pre-Chamber Combustion Characteristics*. https://doi.org/10.4271/2020-01-0821

Smith, G. P., Golden, D. M., Frenklach, M., Moriarty, N. W., Eiteneer, B., Goldenberg, M., Bowman, C. T., Hanson, R. K., Song, S., & Gardiner Jr, W. C. (1999). GRI 3.0 Mechanism. *Gas Research Institute*. http://www.me.berkeley.edu/gri_mech/

Smulter, B. (2016). *Instant loading for gas engines* [Master's Thesis].

Song, R., Vedula, R., Zhu, G., & Schock, H. (2017). A control-oriented combustion model for a turbulent jet ignition engine using liquid fuel. *International Journal of Engine Research*, *19*, 146808741773169. https://doi.org/10.1177/1468087417731698

Summers, C. E. (1926). *Internal Combustion Engine* (Patent No. 1568638).

Tang, Q., Sampath, R., Sharma, P., Marquez, M. E., Cenker, E., & Magnotti, G. (2022). Study on the effects of narrow-throat pre-chamber geometry on the pre-chamber jet velocity using dual formaldehyde PLIF imaging. *Combustion and Flame*, *240*, 111987. https://doi.org/10.1016/j.combustflame.2022.111987

Toulson, E., Schock, H., & Attard, W. (2010, October). A Review of Pre-Chamber Initiated Jet Ignition Combustion Systems. *SAE Technical Papers*. https://doi.org/10.4271/2010-01-2263

Trombley, G., & Toulson, E. (2023). A fuel-focused review of pre-chamber initiated combustion. *Energy Conversion and Management*, *298*, 117765. https://doi.org/10.1016/j.enconman.2023.117765

Turkish, M. C. (1974). 3—Valve Stratified Charge Engines: Evolvement, Analysis and Progression. *SAE Transactions*, *83*, 3483–3503. JSTOR.

United Nations. (2022, March 1). *Causes and effects of climate change*. Climate Action | United Nations. https://www.un.org/en/climatechange/science/causes-effects-climate-change

Watson, H. C. (1997). *Internal combustion engine ignition device* (Patent No. US Patent 5,611,307).

Woschni, G. (1967). A Universally Applicable Equation for the Instantaneous Heat Transfer Coefficient in the Internal Combustion Engine. *SAE Technical Paper*.

Wray, A. P., Ibrahim, S. S., & Carrotte, J. F. (1997). Engineering Thermodynamics. *Departmental Publication No. 18, AAE Department, Loughborough University*.

Zucrow, M., & Hoffman, J. (1976). *Gas Dynamics, vol 1 John Wiley \& Sons*. Hoboken, New Jersey.

Appendices

Appendix 1. Detailed derivation of the HRR equation

Employing the first law of thermodynamics for the MCC volume provides,

$$\frac{dU_{MCC}}{dt} = \frac{dQ_{MCC}}{dt} - P_{MCC}\frac{dV}{dt} + h_{\frac{PCC}{MCC}}\frac{dm}{dt} \tag{1}$$

where $h_{\frac{PCC}{MCC}}$ denotes as the enthalpy transfer between the MCC and the pre-chamber. Similarly, for the PCC employing the first law of thermodynamics,

$$\frac{dU_{PCC}}{dt} = \frac{dQ_{MCC}}{dt} - h_{\frac{PCC}{MCC}}\frac{dm}{dt} \tag{2}$$

$$dU = mc_v dT \tag{3}$$

$$\frac{dU}{dt} = mc_v\frac{dT}{dt} \tag{4}$$

dU represents the changes in the internal energy, and according to the ideal gas law,

$$PV = mRT \tag{5}$$

Differentiating the ideal gas law equation results in,

$$mRdT = VdP + PdV \tag{6}$$

$$\frac{dT}{T} = \frac{dP}{P} + \frac{dV}{V} \tag{7}$$

Again, in Equation (7),

$$\frac{dU}{dt} = mc_v\frac{d}{dt}\left(T\frac{dP}{P} + T\frac{dV}{V}\right) \tag{8}$$

Employing ideal gas law equation here,

$$\frac{dU}{dt} = mc_v \frac{d}{dt}\left(\frac{V}{mR}dP + \frac{P}{mR}dV\right) = \frac{C_V}{R}\ (VdP + PdV) \tag{9}$$

Consequently,

$$\frac{dU}{dt} = \frac{C_V}{R}\left(V\frac{dP}{dt} + P\frac{dV}{dt}\right) \tag{10}$$

Using the Equation 47 in terms of the MCC,

$$\frac{dU_{MCC}}{dt} = \frac{C_V}{R}\left(V_{MCC}\frac{dP_{MCC}}{dt} + P_{MCC}\frac{dV_{MCC}}{dt}\right) \tag{11}$$

Likewise for PCC system,

$$\frac{dU_{PCC}}{dt} = \frac{C_V}{R}\ V_{PCC}\frac{dP_{PCC}}{dt} \tag{12}$$

Here, as the PCC volume is constant ($\frac{dV_{PCC}}{dt} = 0$) whereas the MCC volumes changes because of piston motion.